J. Fluid Mech. (2011), *vol.* 667, *pp.* 555–585.
doi:10.1017/S0022112010004593

Dispersive dam-break and lock-exchange flows in a two-layer fluid

J. G. ESLER† AND J. D. PEARCE

Department of Mathematics, University College London, 25 Gower Street, London WC1E 6BT, UK

(Received 8 February 2010; revised 3 September 2010; accepted 5 September 2010)

Dam-break and lock-exchange flows are considered in a Boussinesq two-layer fluid system in a uniform two-dimensional channel. The focus is on inviscid 'weak' dam breaks or lock exchanges, for which waves generated from the initial conditions do not break, but instead disperse in a so-called undular bore. The evolution of such flows can be described by the Miyata–Camassa–Choi (MCC) equations. Insight into solutions of the MCC equations is provided by the canonical form of their long wave limit, the two-layer shallow water equations, which can be related to their single-layer counterpart via a surjective map. The nature of this surjective map illustrates that whilst some Riemann-type initial-value problems (dam breaks) are analogous to those in the single-layer problem, others (lock exchanges) are not. Previous descriptions of MCC waves of permanent form (cnoidal and solitary waves) are generalised, including a description of the effects of a regularising surface tension. The wave solutions allow the application of a technique due to El's approach, based on Whitham's modulation theory, which is used to determine key features of the expanding undular bore as a function of the initial conditions. A typical dam-break flow consists of a leftwards-propagating simple rarefaction wave and a rightward-propagating simple undular bore. The leading and trailing edge speeds, leading edge solitary wave amplitude and trailing edge linear wavelength are determined for the undular bore. Lock-exchange flows, for which the initial interface shape crosses the mid-depth of the channel, by contrast, are found to be more complex, and depending on the value of the surface tension parameter may include 'solibores' or fronts connecting two distinct regimes of long-wave behaviour. All of the results presented are informed and verified by numerical solutions of the MCC equations.

Key words: internal waves, ocean processes, shallow water flows

1. Introduction

A bore can be defined as a fluid flow connecting two uniform basic states. In the context of single-layer flow, some of the most famous examples include river bores such as those on the Severn (UK) and Dordogne (France). Large amplitude bores tend to be turbulent, and turbulent bores are typically modelled by a localised discontinuity satisfying physically or empirically derived Rankine–Hugionot conditions. For relatively small depth ratios, however, the bore consists of a nonlinear wavetrain and is said to be 'undular' (the early experimental work of Favre 1935 suggests a critical depth ratio for water waves of around 1.28).

† Email address for correspondence: gavin@math.ucl.ac.uk

In this work, the focus is on internal undular bores generated by (partial) dam breaks in a two-layer fluid. Dam breaks may be regarded as the canonical generation mechanism for undular bores, and the dam-break problem is an essential pre-requisite for understanding undular bores in more complex flows, such as those generated by transcritical flow over topography (e.g. El, Grimshaw & Smyth 2009). The present study is motivated by the ever increasing number of observations revealing the ubiquity of internal undular bores in the atmosphere (e.g. Clarke 1998; Rottman & Grimshaw 2002), where they may influence local weather events (e.g. thunderstorm initiation), as well as in the coastal oceans (e.g. Holloway, Pelinovsky & Talipova 2001; Grimshaw 2002), where they have a role in mixing processes and in the energy budgets of tidal flows.

The typical situation to be considered is shown in figure 1(a,b), which illustrates schematically how a typical dam break initial condition evolves into a rightward-propagating undular bore and leftward-propagating 'rarefaction wave'. The somewhat more complicated situation of a lock-exchange flow, which occurs in the two-layer system but not in the single-layer one, is illustrated in figure 1(c,d). Understanding how and why the development of the lock exchange differs from the dam break will be a key focus below. An assumption made throughout the present work is that the dam breaks considered are sufficiently weak, in the sense of the interface height difference across the barrier being small (in some sense), and are initialised sufficiently smoothly, that no wave breaking results. Based on this assumption, a suitable model is the Miyata–Choi–Camassa (MCC) equations (following Miyata 1985; Choi & Camassa 1999). The MCC equations are an extension of the two-layer shallow water equations (SWE hereafter) with additional regularising dispersive terms which preclude wave breaking entirely. Therefore, the results below are complementary to previous analytical, experimental and numerical studies of dam breaks, lock exchanges (e.g. Klemp, Rotunno & Skamarock 1997; Shin, Dalziel & Linden 2005) and gravity currents (e.g. Benjamin 1968; Rottman & Simpson 1983; Klemp, Rotunno & Skamarock 1994) in two-layer fluids. In the aforementioned studies, the focus has been on 'strong' dam breaks, which include gravity currents as a special case, in which wave breaking is observed (or assumed) and the internal bores are turbulent. There has been much discussion in the literature about the appropriate Rankine–Hugoniot conditions to apply at an internal bore or gravity current in a two-fluid system. Possible jump conditions follow from the assumption of no energy dissipation in the contracting layer (Chu & Baddour 1977; Wood & Simpson 1984), or the opposite extreme that no energy dissipation occurs in the expanding layer. Theoretical (Li & Cummins 1998) and experimental (Baines 1984; Rottman & Simpson 1989) results indicate that spatially localised internal bores must propagate at speeds between the values predicted by the above two hypotheses. In the present study, by contrast, we will be concerned with undular bores which do not break and do not remain localised.

In single-layer flows the study of undular bores has followed Benjamin & Lighthill (1954), who considered the steady undular bores that result when dissipation is present, and Gurevich & Pitaevskii (1974), who solved a model 'dam break' initial-value problem in the absence of dissipation. Both approaches exploit the assumption of weak nonlinearity to derive solutions based on the cnoidal and solitary wave solutions of the Korteweg–de Vries (KdV) equation. The dissipationless case can be argued to be more fundamental, both as a description of the early time behaviour of an undular bore before significant dissipation occurs, and as a generic paradigm relevant to many branches of physics. The Gurevich–Pitaevskii solution is based on Whitham modulation theory (following Whitham 1965), for which a scale separation is assumed between

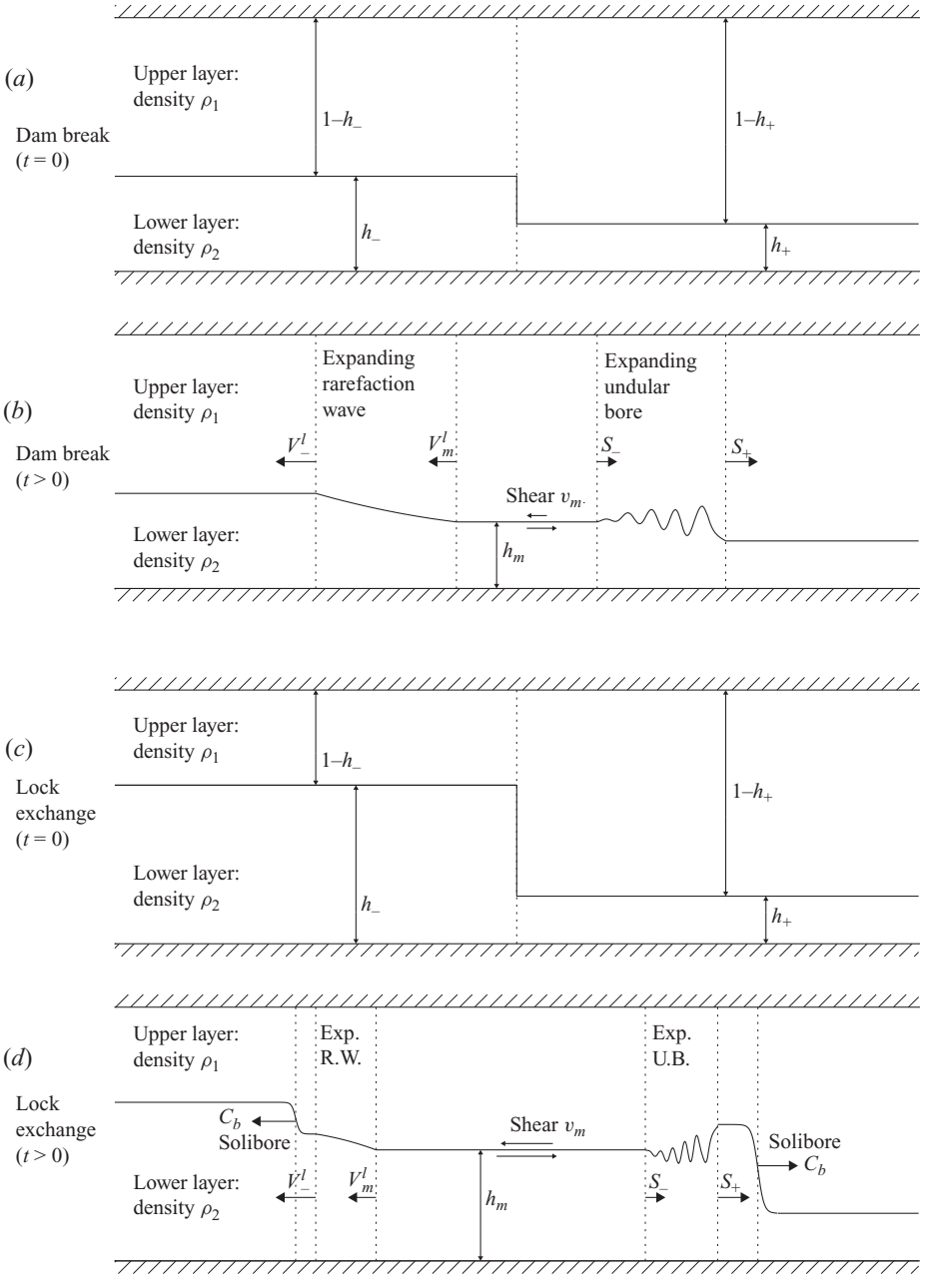

FIGURE 1. (*a*) Dam break $t = 0$: illustrating the physical set-up and step-like initial conditions including definitions of the left and right interface heights h_- and h_+. (*b*) Dam break $t > 0$: schematic illustration of a typical developing undular bore and rarefaction wave, including the definition of the undular bore leading and trailing edge speeds s_+ and s_-, the mid-state $(v, h) = (v_m, h_m)$ and long wave speeds V_+^l and V_m^l associated with the boundaries of the rarefaction wave. (*c*) Lock exchange $t = 0$: the initial conditions for a lock exchange cross the mid-depth of the channel. (*d*) Lock exchange $t > 0$: schematic illustration of a typical lock-exchange development including solibores.

the variation of mean quantities and a typical cnoidal wavelength. A consequence of the integrability of the KdV equation is that the resulting modulation equations may be obtained in Riemann invariant form and integrated to obtain full analytical expressions for the variation of mean physical quantities across the undular bore.

Undular bores are generic features of nonlinear hyperbolic systems regularised by (weak) dispersion, such as the MCC equations discussed above. Unlike the KdV, however, the MCC equations, and their associated modulation equations, are not thought to be integrable. Until recently, it was unclear how the Gurevich–Pitaevskii approach could be usefully extended to non-integrable systems. However, El (2005) (see also El, Khodorovskii & Tyurina 2003, 2005) have demonstrated that insights from Whitham modulation theory can be used to determine details of undular bores in a wide class of non-integrable hyperbolic equations supporting bidirectional wave propagation. El's (and co-authors') technique allows simple undular bores to be 'fit' into solutions of the underlying long wave equations, much as localised jump discontinuities are fit into solutions of the SWE as models of turbulent bores in the classical dam-break problem.

A dissipationless undular bore differs from its localised turbulent counterpart in that respect as it occupies a uniformly expanding region between a leading (e.g. solitary wave) edge with speed s_+ and a trailing (e.g. linear wave) edge with speed s_-, as illustrated in figure 1. Using El's technique, an explicit resolution of the details of the undular bore is not necessary to obtain key quantities, such as the propagation speeds of the boundaries of the undular bore (s_- and s_+), the leading edge solitary wave amplitude and the trailing edge linear wavenumber. The application of El's technique to a wide class of systems supporting bidirectional wave propagation, which will be shown below to include the MCC, is discussed in detail in El (2005, § 5), as well as in El *et al.* (2005). The main points of their arguments will be reviewed below. A successful application of El's technique to dam breaks in the single-layer Su–Gardner (Su & Gardner 1969) dispersive shallow water model is described in El, Grimshaw & Smyth (2006). Details of the single-layer dam-break solution were essential pre-requisites for solution of the important physical problem of near-critical flow over topography in the dispersive regime (El *et al.* 2009).

The objective of the present work is to apply El's technique to two-layer dam breaks and lock exchanges. In § 2, the physical problem to be addressed is described together with the MCC equations used to model the resulting fluid flows. The conservation properties of the MCC are stated and the properties of the equations in the long wave (SWE) limit are reviewed. A formal distinction is made between generalised 'dam break' and 'lock-exchange' initial conditions. In § 3, a general treatment of the steadily propagating wave solutions of the MCC is presented. Previous results for solitary wave speeds are generalised to allow for arbitrary vertical shears and the properties of the 'solibore' solution of the MCC are reviewed. Section 4 considers the dam-break problem, and it is demonstrated how El's technique can be used to 'fit' undular bores into solutions of the two-layer SWE. In § 5, the predictions of El's technique are compared with numerical simulations of both dam-break and lock-exchange flows as described by the MCC equations. Finally, in § 6, conclusions are drawn.

2. A dispersive model for internal dam-break and lock-exchange flows

2.1. *The physical problem*

Figure 1 illustrates the initial conditions for the general physical situation of interest. A uniform infinite two-dimensional channel of height H contains two fluids of densities

ρ_1 and ρ_2. For ease of exposition, the Boussinesq approximation $\Delta = (\rho_2 - \rho_1)/2(\rho_2 + \rho_1) \ll 1$ is assumed in all that follows (the non-Boussinesq case is discussed by Choi & Camassa 1999). At $t = 0$ the initial conditions are taken to be step-like as illustrated in figure 1, and the system evolves freely for $t > 0$, creating a dispersive 'dam-break' or 'lock-exchange' flows.

The validity of the analysis to follow depends upon a further assumption. The wave field developing from the step-like initial condition must not include steep or breaking waves, as the validity of the MCC set depends upon a shallowness parameter remaining small. Strictly speaking the step-like initial condition of figure 1, with infinite gradients in interface height, is invalid from the outset. However, asymptotic solutions derived from Whitham modulation theory are valid only at times which are sufficiently long to allow the development of a separation of scales between the modulation scale of the wave envelope and a typical wavelength. It follows that the initial conditions need only resemble a step-like discontinuity on the long modulation scale for the analysis to be asymptotically valid. The modulation scale itself increases linearly with time, so the wave envelope evolving from any smoothed step will eventually resemble the formal solution evolving from the discontinuous step. Consequently, an experimental set-up aimed at investigating internal undular bores might, therefore, be initialised with a 'smoothed-step' profile to prevent wave-breaking at early times from inhibiting the development of an undular bore.

2.2. *The Miyata–Choi–Camassa equations*

The Miyata–Choi–Camassa equations are a dispersive two-layer set that remain valid for low wave slopes, but allow for strong nonlinearity. For Boussinesq flow in a channel of unit depth as described above, the non-dimensional MCC equations are

$$\left.\begin{aligned} u_{1t} + u_1 u_{1x} &= -\Pi_x + \frac{1}{3h_1}\left(h_1^3 \mathscr{G}[u_1]\right)_x, \\ u_{2t} + u_2 u_{2x} &= -\Pi_x - h_{2x} + \frac{1}{3h_2}\left(h_2^3 \mathscr{G}[u_2]\right)_x + \tau h_{2xxx}, \\ h_{1t} + (u_1 h_1)_x &= 0, \\ h_{2t} + (u_2 h_2)_x &= 0, \end{aligned}\right\} \tag{2.1}$$

where u_1, u_2 are the layer-averaged velocities in the upper and lower layers, respectively, h_1 and h_2 are the corresponding layer thicknesses and Π is the pressure at either a free upper surface or at the rigid lid (which result in equivalent systems in the Boussinesq limit). All lengths are scaled on the channel depth H so that in (2.1) $0 \leqslant h_1, h_2 \leqslant 1$, velocities are scaled on $c = \sqrt{\Delta g H}$ and pressures on c^2. The nonlinear differential operator $\mathscr{G}[\cdot]$ acts on a given function $f(x, t)$ as follows:

$$\mathscr{G}[f] = f_{xt} + f f_{xx} - (f_x)^2. \tag{2.2}$$

The non-dimensional parameter $\tau = \gamma/\rho_0 g' H^2$, where γ is the dimensional surface tension, is an inverse Bond number. The surface tension terms in (2.1) have been linearised under the assumption of small interface curvature, an approximation which is justified as it is consistent with the regime of validity of the MCC itself (small aspect ratio). Finite surface tension (or some other mechanism) is necessary to regularise the MCC equations with respect to the MCC analogue of Kelvin–Helmholtz instability (e.g. Liska, Margolin & Wendroff 1995), for which there is no short-wave cutoff. In the absence of surface tension, short waves are invariably unstable in the presence of shear between the layers. With regards to the oceanographic application discussed above, the surface tension cannot be justified physically, and is perhaps best considered as a

numerical filter that is required for regularisation. Note that an alternative approach to regularisation has been described recently by Choi, Barros & Jo (2009). Nevertheless, τ is retained throughout our analysis since there is no obstacle in principle to setting up experiments in a two-fluid system with finite τ, with which the results below might be compared.

The final two equations in (2.1) can be combined and integrated to give

$$u_1(1-h)+u_2h=M(t), \tag{2.3}$$

where $M(t)$ is the total momentum of the flow. In the absence of fixed topography and external body forces it is possible to set $M\equiv 0$ and work in the frame in which the total momentum is zero, without loss of generality. The unknown upper surface pressure Π can then be eliminated from the equations by introducing a baroclinic velocity, v, and interface height, h,

$$v=u_2-u_1, \quad h=h_2. \tag{2.4}$$

The MCC equations can then be written as

$$\left.\begin{aligned} h_t+(vh(1-h))_x&=0,\\ v_t+\left(\frac{1}{2}v^2(1-2h)+h\right)_x&=\tau h_{xxx}+\frac{\left(h^3\mathscr{G}[v(1-h)]\right)_x}{3h}-\frac{\left((1-h)^3\mathscr{G}[-vh]\right)_x}{3(1-h)}\end{aligned}\right\}. \tag{2.5}$$

The step-like initial conditions illustrated in figure 1 are

$$v(x,0)=\begin{cases}v_- & x<0,\\ v_+ & x>0,\end{cases} \qquad h(x,0)=\begin{cases}h_- & x<0,\\ h_+ & x>0,\end{cases} \tag{2.6}$$

and define the so-called Gurevich–Pitaevskii problem, to be addressed in §§ 4 and 5, respectively.

2.3. *Conservation properties of the Miyata–Choi–Camassa equations*

The set (2.5) can be obtained from direct approximation of the Hamiltonian of the two-layer Euler equations, and consequently satisfy various laws related to those of the full system (Choi & Camassa 1999). Transformation to the frame with $M=0$ implies automatic conservation of total momentum, hence the expected conservation laws are for mass, 'irrotationality' (corresponding to conservation of depth-integrated x–z vorticity) in the upper and lower layers and total energy. For the modulation theory presented in § 4, it is advantageous to write the conservation laws in 'flux form' using only the dependent variables (v,h) (see e.g. Kamchatnov 2000).

The flux form of the mass conservation law is

$$\mathscr{M}_t+\mathscr{V}_x=0, \tag{2.7}$$

where $\mathscr{M}\equiv h$ and $\mathscr{V}=vh(1-h)$, i.e. the first of the MCC equations (2.5). The remaining conservation laws are, after some manipulation, found to be

$$\left.\begin{aligned} \mathscr{I}_{1t}+\mathscr{J}_{1x}&=0, \quad \text{(upper layer irrotationality)},\\ \mathscr{I}_{2t}+\mathscr{J}_{2x}&=0, \quad \text{(lower layer irrotationality)},\\ \mathscr{E}_t+\mathscr{F}_x&=0, \quad \text{(energy)},\end{aligned}\right\} \tag{2.8}$$

with the conserved quantities $\mathscr{I}_i$ $(i=1,2)$ and their fluxes $\mathscr{J}_i$ given by

$$\mathscr{I}_1=u_1+\tfrac{1}{6}(1-h)^2u_{1xx}, \quad \mathscr{J}_1=\Pi+\tfrac{1}{2}u_1^2-\tfrac{1}{6}(1-h)^2(\mathscr{G}[u_1]+u_1u_{1xx}), \tag{2.9}$$

$$\mathscr{I}_2=u_2+\tfrac{1}{6}h^2u_{2xx}, \quad \mathscr{J}_2=\Pi+h+\tfrac{1}{2}u_2^2-\tau h_{xx}-\tfrac{1}{6}h^2(\mathscr{G}[u_2]+u_2u_{2xx}). \tag{2.10}$$

The two irrotationality relations can be combined by writing $\mathscr{I} = \mathscr{I}_2 - \mathscr{I}_1$ and $\mathscr{J} = \mathscr{J}_2 - \mathscr{J}_1$ into a single relation involving only v, h and their derivatives

$$\mathscr{I}_t + \mathscr{J}_x = 0, \tag{2.11}$$

where

$$\mathscr{I} = v + \tfrac{1}{6} v_{xx} h(1-h) + \tfrac{1}{6}(1-2h)(2v_x h_x + v h_{xx}), \tag{2.12}$$

and

$$\mathscr{J} = h + \tfrac{1}{2} v^2 (1-2h) + \tfrac{1}{2}(1-h)^2 \mathscr{G}[-vh] - \tfrac{1}{2} h^2 \mathscr{G}[v(1-h)] - \tfrac{1}{6} vh(1-h)(2v_x h_x + h_{xx}) - \tau h_{xx}. \tag{2.13}$$

The energy density, $\mathscr{E}$, and its flux, $\mathscr{F}$, are given by

$$\mathscr{E} = \tfrac{1}{2}\tau h_x^2 - \tfrac{1}{2}(1-v^2)h(1-h) + \tfrac{1}{6}\left(v_x^2 h^2 (1-h)^2 + 2v_x h_x v h(1-h)(1-2h) + (1-3h(1-h))v^2 h_x^2\right), \tag{2.14}$$

and

$$\mathscr{F} = -\tfrac{1}{2} vh(1-h)(1-v^2)(1-2h) + \tau h_x (vh(1-h))_x - \tfrac{1}{3} vh(1-h) \times \left\{h^2 \mathscr{G}[v(1-h)] - (1-h)^2 \mathscr{G}[-vh] + v_x h_x v h(1-h) + 2(1-2h)v^2 h_x^2 + 3\tau h_{xx}\right\}. \tag{2.15}$$

The three conservation laws (2.7)–(2.11) are required for the Whitham modulation theory to be presented in § 4.

2.4. *The long wave limit: the two-layer shallow water equations*

Before using El's technique to investigate undular bore solutions of the MCC equations, it is necessary to have a clear understanding of the behaviour of the MCC in the long wave limit, described by the two-layer SWE

$$\boldsymbol{h}_t + \boldsymbol{A}\boldsymbol{h}_x = 0, \quad \text{where } \boldsymbol{h} = \begin{pmatrix} v \\ h \end{pmatrix}, \quad \boldsymbol{A} = \begin{pmatrix} v(1-2h) & 1-v^2 \\ h(1-h) & v(1-2h) \end{pmatrix}. \tag{2.16}$$

Equation (2.16) is simply the MCC equations (2.5) with dispersive and surface tension terms neglected, as is consistent with the long wave limit. It is straightforward (e.g. Cavanie 1969; Sandstrom & Quon 1993; Baines 1995; Milewski *et al.* 2004) to write (2.16) in canonical Riemann invariant form. The result is

$$\left[\frac{\partial}{\partial t} + \left(v(1-2h) \pm \left[h(1-h)(1-v^2)\right]^{1/2}\right)\frac{\partial}{\partial x}\right]\left(v(1-2h) \pm 2\left[h(1-h)(1-v^2)\right]^{1/2}\right) = 0. \tag{2.17}$$

There are several points to note as follows.

(*a*) A necessary condition for (2.16) to remain hyperbolic is $|v| < 1$. The canonical form of (2.16) reveals that if initially $|v| < 1$ everywhere in the fluid then it will remain so, at least up to the occurrence of wave breaking (e.g. Milewski *et al.* 2004; Zahibo *et al.* 2007). Where $|v| > 1$ the fluid is unstable to a (long-wave) shear instability. Notwithstanding the nomenclature adopted elsewhere in the literature, the two-layer SWE shear instability is not directly related to the Kelvin–Helmholtz instability of a two-layer fluid, which is a short-wave instability and consequently is excluded by construction from the SWE. Both the long-wave shear and Kelvin–Helmholtz

instabilities are present for linear waves in the MCC system, albeit with the latter in a modified form.

(*b*) A remarkable result has been noted by Chumakova *et al.* (2009). The canonical form (2.17) *appears* to be exactly identical to that of the single-layer SWE. The single-layer SWE can be written, for velocity u and layer thickness σ, in the form

$$\left[\frac{\partial}{\partial t} + \left(u \pm \sigma^{1/2}\right)\frac{\partial}{\partial x}\right]\left(u \pm 2\sigma^{1/2}\right) = 0, \tag{2.18}$$

hence there exits a mapping $v(1-2h) \equiv U \to u$, $h(1-h)(1-v^2) \equiv \Sigma \to \sigma$ between the two systems. Consequently, both systems can be recast as

$$\left[\frac{\partial}{\partial t} + \left(\frac{3}{4}L + \frac{1}{4}R\right)\frac{\partial}{\partial x}\right]L = 0, \quad \left[\frac{\partial}{\partial t} + \left(\frac{3}{4}R + \frac{1}{4}L\right)\frac{\partial}{\partial x}\right]R = 0, \tag{2.19}$$

in terms of their respective Riemann invariants L, R. Explicitly, for the two-layer system these are

$$\left.\begin{aligned} L &= v(1-2h) - 2\left[h(1-h)(1-v^2)\right]^{1/2}, \\ R &= v(1-2h) + 2\left[h(1-h)(1-v^2)\right]^{1/2}, \end{aligned}\right\} \tag{2.20}$$

with the corresponding long wave speeds $V^l = (3L+R)/4$ and $V^r = (L+3R)/4$ given by

$$\left.\begin{aligned} V^l &= v(1-2h) - \left[h(1-h)(1-v^2)\right]^{1/2}, \\ V^r &= v(1-2h) + \left[h(1-h)(1-v^2)\right]^{1/2}. \end{aligned}\right\} \tag{2.21}$$

(*c*) The mapping $(U, \Sigma) \to (u, \sigma)$ suggests a close relationship between solutions of the two-layer SWE and its single-layer counterpart. However, the relationship cannot be as straightforward as a one-to-one mapping, as suggested by Chumakova *et al.* (2009). Physically, the reason for this is that there is no single-layer counterpart to a 'lock-exchange' flow in a two-layer fluid, in which the initial interface profile is a step spanning the centre of the fluid domain. Lock-exchange experiments (e.g. Shin *et al.* 2005), reveal that such flows evolve into two gravity currents propagating in each direction within the fluid, a situation which has no single-layer counterpart. Mathematically, the important point is that the mapping $(U, \Sigma) \to (u, \sigma)$ is surjective, but not injective with respect to the original two-layer variables (v, h). In fact, generally, for fixed (u, σ) *four* different values of (v, h) will map to that value of (u, σ). This is partly accounted for by the obvious up–down symmetry $h \to 1-h$, $v \to -v$, but another less obvious symmetry is

$$v \to 1-2h, h \to \frac{1-v}{2}. \tag{2.22}$$

We will refer to the mapping from (v, h) to (u, σ) as the 'St Andrew's Cross' mapping, because the mapping divides up the rectangular (v, h) domain ($[-1, 1] \times [0, 1]$) along the diagonals of the rectangle (thus resembling the flag of Scotland). The Riemann invariants L and R are contoured as functions of (v, h) in figure 2(*a*), and attain their extreme values along the ascending and descending diagonals, respectively, dividing the (v, h) domain as described.

The surjective 'St Andrew's Cross' map, and specifically the $v \to 1-2h$, $h \to (1-v)/2$ symmetry inherent within it, leads to the conclusion that at a given location the two-layer shallow water system is in one of the two physically different (but mathematically

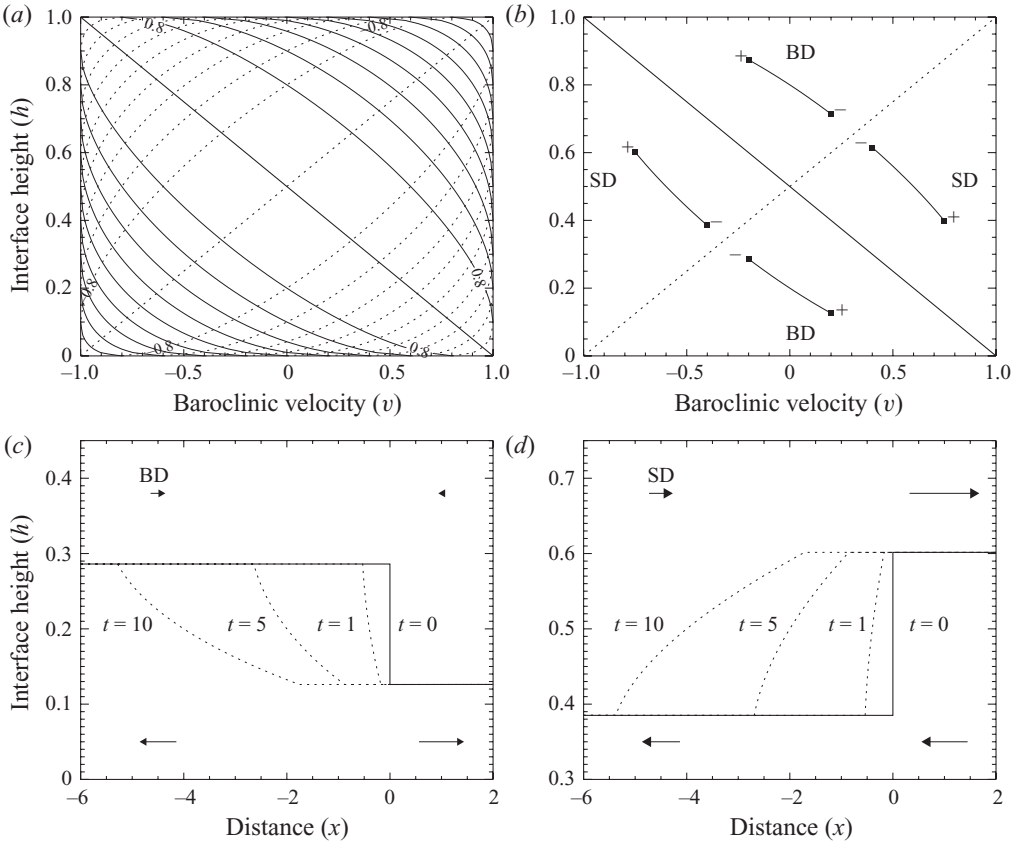

FIGURE 2. (*a*) Contour plot of the Riemann invariants $R(v,h)$ (solid curves) and $L(v,h)$ (dotted curves). (*b*) Possible right (+) and left (−) initial states for a simple leftward-travelling rarefaction waves in the buoyancy dominated (BD) and shear-dominated (SD) regimes. The end states must lie on contours of constant $R(v,h)$ (solid curves). (*c*) The evolution of the interface height $h(x,t)$ during the development of a rarefaction wave in the buoyancy dominated regime. The length of the arrows are proportional to the initial velocities in each layer. (*d*) As (*c*), but for the shear-dominated regime.

identical) states. The first state is 'buoyancy-dominated' with $|v| < |1-2h|$ and the second 'shear-dominated' with $|v| > |1-2h|$. Flows which are everywhere in a single state are analogous to flows in the single-layer system. For these flows, a one-to-one mapping to the single-layer system can be used following the arguments of Chumakova *et al.* (2009). Flows which switch between states, however, are unique to the two-layer system.

(*d*) The two-layer SWE are not *genuinely nonlinear* for all values of (v,h) as the characteristic velocities do not vary monotonically in the direction of the right eigenvectors of $\boldsymbol{A}$. A straightforward calculation reveals that for the rightward-characteristic velocity V^r,

$$\begin{aligned} \boldsymbol{r}_r \cdot \nabla_{\boldsymbol{h}} V^r &= \tfrac{3}{2}(1-2h)\sqrt{1-v^2} - 3v\sqrt{h(1-h)}, \\ &= 0, \quad \text{when} \quad v = (1-2h). \end{aligned} \tag{2.23}$$

Here, $\nabla_{\boldsymbol{h}}$ denotes the gradient operator in (v,h) space and $\boldsymbol{r}_r = (\sqrt{1-v^2} \;\; \sqrt{h(1-h)})^{\mathrm{T}}$ is the right eigenvector associated with V^r. The significance of $\boldsymbol{r}_r$ is that it is everywhere

orientated in the direction in which L is constant, i.e. it is tangent to the integral curves of $L(v, h)$. It is easily verified that $\boldsymbol{r}_r \cdot \boldsymbol{\nabla}_{\boldsymbol{h}} L = 0$ everywhere. The result that $\boldsymbol{r}_r \cdot \boldsymbol{\nabla}_{\boldsymbol{h}} V^r = 0$ along the $R = 1$ diagonal of the St Andrews cross (with $v = 1 - 2h$) implies that within a rightward-propagating simple wave (with L constant everywhere) the long wave speed V^r takes an extreme value there (in this case a maximum). This breakdown of genuine nonlinearity has important consequences for the construction of simple waves of rarefaction, to be discussed below.

The above observations prompt the following definitions.

(*a*) A generalised dam-break flow: A flow that develops from step-like initial conditions (2.6) for which the end states (v_-, h_-) and (v_+, h_+) are located within the same quadrant of the St Andrew's cross. Based on the quadrant, generalised dam breaks can be classified as being either 'buoyancy-dominated' or 'shear-dominated'.

(*b*) A generalised lock-exchange flow: A flow that develops from step-like initial conditions (2.6) for which the end states (v_-, h_-) and (v_+, h_+) are located within different quadrants of the St Andrew's cross.

2.5. *Simple wave solutions in the shallow water limit*

Important and well-known 'simple wave' solutions of (2.17) can be obtained by setting one of the Riemann invariants to be a constant everywhere in the flow. The evolution is then governed by a Hopf equation for the remaining Riemann invariant, which has well-known solutions featuring wave steepening and breaking within a finite time (e.g. Zahibo *et al.* 2007).

A special case, which will be of significance below, is that of the centred 'rarefaction wave'. Consider step-like initial conditions (2.6) satisfying

$$R(v_-, h_-) = R(v_+, h_+) = R_0, \quad L(v_-, h_-) = L_-, \quad L(v_+, h_+) = L_+, \tag{2.24}$$

with $L_- < L_+$, and with both (v_-, h_-) and (v_+, h_+) located within the same quadrant of the St Andrew's cross. The four possibilities for such an initial condition are illustrated in figure 2(*b*). Clearly $R(x, t) = R_0$ for all time, whereas $L(x, t)$ is governed by

$$\left(\partial_t + \left(\tfrac{3}{4}L + \tfrac{1}{4}R_0\right)\partial_x\right) L = 0, \tag{2.25}$$

which has solution

$$L(x,t) = \begin{cases} L_-, & x/t < \tfrac{3}{4}L_- + \tfrac{1}{4}R_0, \\ 4x/3t - R_0/3, & \tfrac{3}{4}L_+ + \tfrac{1}{4}R_0 > \quad x/t > \tfrac{3}{4}L_- + \tfrac{1}{4}R_0, \\ L_+, & x/t > \tfrac{3}{4}L_+ + \tfrac{1}{4}R_0. \end{cases} \tag{2.26}$$

which is a leftwards-propagating centred rarefaction wave.

Care must be taken in obtaining explicit expressions for $v(x, t)$ and $h(x, t)$ in terms of R_0, L_- and L_+, due to the multi-valued nature of the mapping from the Riemann invariants to v and h. The quantity $H = h(1 - h)$ can be recovered from (L, R) using

$$H(L, R) = \tfrac{1}{8}\left((1 - LR) \pm [(1 - L^2)(1 - R^2)]^{1/2}\right), \tag{2.27}$$

where the positive sign for the square root is chosen when working in a 'shear-dominated' quadrant and the negative sign for a 'buoyancy-dominated' quadrant. The two solutions of the quadratic $h(1-h) = H$ (i.e. $h = 1/2 \pm \sqrt{1/4 - H}$) correspond to the up–down symmetry in the problem.

Figures 2(*c*) and 2(*d*) show examples of simple leftward-propagating rarefaction waves resulting from Riemann problem initial conditions with $R = R_0 = 0.8$ everywhere, and with $L_- = -0.971$ and $L_+ = -0.501$. The four possible locations in

(v, h) space of the end points with these Riemann invariants are shown in figure 2(b). Figure 2(c) shows a developing rarefaction example from the buoyancy-dominated regime and figure 2(d) from the shear-dominated regime.

The case, where (v_-, h_-) and (v_+, h_+) lie with different quadrants of the St Andrew's cross, with $R_- = R_+ = R_0$ constant, must be considered separately. As discussed above, genuine nonlinearity of the two-layer SWE breaks down at the diagonal (in this case the $L = -1$, $v = -(1-2h)$ diagonal). The corresponding maximum in the wave speed (here V^l) implies that the construction of a simple wave of rarefaction cannot be continued across the diagonal, where the wave slope would become infinite. The conclusion is that states with in $R_- = R_+ = R_0$, located in opposite quadrants of the St Andrew's cross diagram must be connected by *compound waves*. Compound waves are purely leftward- or rightward-propagating waves that are composed of both rarefactions and (dispersive or dissipative) shocks, and are analogous to those in single variable nonlinear hyperbolic systems with non-convex flux functions, such as the Buckley–Leverett equation (Buckley & Leverett 1942).

3. Steadily propagating wave solutions of the MCC equations

Choi & Camassa (1999) have shown that the MCC equations (2.5) support travelling waves of permanent form. For the purposes of the modulation theory below, it is necessary to significantly adapt and extend Choi and Camassa's results, notably for consistency with the two variable (v, h) picture presented above.

3.1. *Waves of permanent form: general case*

Consider waves propagating steadily at speed c, so that $\partial_t \to -c\partial_x$. The mass conservation MCC equation can then be integrated to give

$$v = \frac{c(h-h_*)}{h(1-h)}, \tag{3.1}$$

where the constant h_* may be interpreted as the 'level of zero shear' for the particular flow supporting the waves. The MCC velocity equation can now be written as

$$\left(-\frac{c^2(h-h_*)}{h(1-h)} + \frac{c^2(1-2h)}{2}\left(\frac{h-h_*}{h(1-h)}\right)^2 + h\right)_x = \tau h_{xxx} - \frac{c^2h_*^2}{3h}\left(h\left(\frac{h_x}{h}\right)_x\right)_x - \frac{c^2(1-h_*)^2}{3(1-h)}\left((1-h)\left(\frac{h_x}{1-h}\right)_x\right)_x, \tag{3.2}$$

where the identity

$$\mathscr{G}[f] = (f-c)^2\left(\frac{(f-c)_x}{f-c}\right)_x, \tag{3.3}$$

for any $f(x-ct)$ has been used. Integrating in x and rearranging gives

$$\frac{\mathrm{d}}{\mathrm{d}h}\left(\frac{c^2(h-h_*)^2}{2h(1-h)}\right) - h + \frac{b_1}{2} = \frac{1}{6}\frac{\mathrm{d}}{\mathrm{d}h}\left(\frac{c^2(h_x)^2(h_*^2+(1-2h_*)h)}{h(1-h)} - 3\tau(h_x)^2\right), \tag{3.4}$$

where b_1 is an arbitrary constant of integration. The equation can now be integrated with respect to h and rearranged to give

$$(h_x)^2 = \frac{3\left[h^4 - (1+b_1)h^3 + (c^2+b_1-b_2)h^2 + (b_2-2c^2h_*)h + c^2h_*^2\right]}{c^2h_*^2 + c^2(1-2h_*)h - 3\tau h(1-h)} = \frac{3P(h)}{N(h)}, \tag{3.5}$$

where b_2 is a second constant of integration.

The quartic polynomial $P(h)$ appearing in the numerator of (3.5) can be written as

$$P(h) = (h - h_1)(h - h_2)(h - h_3)(h - h_4), \tag{3.6}$$

introducing the four (possibly complex) roots h_i $(i = 1, 2, 3, 4)$. Equating coefficients, and eliminating the unknown constants b_1, b_2, reveals the following relations between the roots h_i, the wave speed, c, and the zero shear level, h_*:

$$\left.\begin{aligned} h_1h_2h_3h_4 &= c^2h_*^2, \\ (1-h_1)(1-h_2)(1-h_3)(1-h_4) &= c^2(1-h_*)^2. \end{aligned}\right\} \tag{3.7}$$

Clearly, the h_i must be either real or form complex conjugate pairs. In either case the denominator in (3.5) can be written as

$$N(h) = h_1h_2h_3h_4(1-h) + (1-h_1)(1-h_2)(1-h_3)(1-h_4)h - 3\tau h(1-h). \tag{3.8}$$

Rearrangement of (3.7) allows c and h_* to be expressed in terms of the roots h_i

$$h_* = \frac{\sqrt{h_1h_2h_3h_4}}{\sqrt{h_1h_2h_3h_4} + \sqrt{(1-h_1)(1-h_2)(1-h_3)(1-h_4)}}, \tag{3.9}$$

$$c = \pm\left(\sqrt{h_1h_2h_3h_4} + \sqrt{(1-h_1)(1-h_2)(1-h_3)(1-h_4)}\right). \tag{3.10}$$

It is notable that both c and h_* have an elementary dependence on the roots h_i that does not directly involve the surface tension parameter, τ. It is also possible to express v in terms of h and the roots h_i by substituting (3.9)–(3.10) back into (3.1)

$$v = \pm\frac{h\sqrt{(1-h_1)(1-h_2)(1-h_3)(1-h_4)} - (1-h)\sqrt{h_1h_2h_3h_4}}{h(1-h)}, \tag{3.11}$$

where the positive sign corresponds to rightward-propagating waves and the negative sign to leftward-propagating waves.

Three possibilities are now considered for wave-like solutions of (3.5).

(*a*) Low surface tension case. The roots h_i are real and ordered $(h_1 \leqslant h_2 \leqslant h_3 \leqslant h_4)$ and $N(h) > 0$ for $h \in [h_2, h_3]$. Inspection of $N(h)$ reveals that such waves will exist only for sufficiently low surface tension (low τ). Waves exist between levels $h = h_2$ and $h = h_3$, with peak-to-trough amplitude $a = h_3 - h_2$ and with wavelength, k, given by

$$\frac{\pi}{k} = \frac{1}{\sqrt{3}}\int_{h_2}^{h_3} \frac{\sqrt{N(h)}}{\sqrt{P(h)}}\,\mathrm{d}h. \tag{3.12}$$

It follows from the positivity of the right-hand sides of (3.7) that $0 \leqslant h_1, h_2, h_3, h_4 \leqslant 1$. A sufficient condition to guarantee $N(h) > 0$ throughout $h \in [0, 1]$ can be obtained under the assumption that h_1 and h_4 do not coincide with the boundaries. It follows that $N(0), N(1) > 0$ and therefore that the condition $N(h_c) > 0$, where

$$h_c = \frac{1}{2} + \frac{h_1h_2h_3h_4 - (1-h_1)(1-h_2)(1-h_3)(1-h_4)}{6\tau}, \tag{3.13}$$

is the location of the minimum of $N(h)$, will guarantee $N(h) > 0$ for $h \in [0, 1]$. The condition $N(h_c) > 0$ translates straightforwardly into a condition on τ as

$$\tau < \tau_c' = \frac{1}{3}\left(\sqrt{h_1h_2h_3h_4} + \sqrt{(1-h_1)(1-h_2)(1-h_3)(1-h_4)}\right)^2 = \frac{c^2}{3}. \tag{3.14}$$

The critical condition $\tau_c' = c^2/3$ has been obtained previously (e.g. Laget & Dias 1997) as the boundary between regimes in which weakly nonlinear solitary waves relative

to a stationary background in the two-layer Euler system have opposite polarities. Weakly nonlinear solitary waves are described by the KdV equation and passing through $\tau = \tau_c'$ corresponds to a change in sign of the coefficient of the dispersive term. The weakly nonlinear (KdV) limit is contained within the MCC equations, with the extended KdV equation resulting if the expansion is made close to the diagonals of the St Andrew's cross. Here, however, it has been shown that essentially the same condition on τ extends to all permanent wave solutions of the MCC.

(*b*) High surface tension case I. The h_i are real and ordered and $N(h) < 0$ for $h \in [h_1, h_2]$, or alternatively, the image of these waves under the up–down symmetry (with $N(h) < 0$ for $h \in [h_3, h_4]$). For the former case $a = h_2 - h_1$ and

$$\frac{\pi}{k} = \frac{1}{\sqrt{3}} \int_{h_1}^{h_2} \frac{\sqrt{-N(h)}}{\sqrt{-P(h)}}\, \mathrm{d}h. \tag{3.15}$$

A necessary and sufficient condition for $N(h) < 0$ for $h \in [h_1, h_2]$ is

$$\tau > \tau_c^* = \frac{c^2}{3} \times \max_{i=1,2} \left\{ \frac{h_*^2}{h_i} + \frac{(1-h_*)^2}{1-h_i} \right\}. \tag{3.16}$$

The expression in brackets to be maximised is greater than unity, so it is clear that there is no overlap with the low surface tension regime. In fact, there is an interval $\tau \in [\tau_c', \tau_c^*]$ within which the existence of waves from either regime cannot be guaranteed.

(*c*) High surface tension case II. For this case $N(h) < 0$ for $h \in [h_1, h_4]$ with h_1, h_4 real, but h_2 and h_3 are a complex conjugate pair (with $h_1 \leqslant \mathrm{Re}\{h_2\} = \mathrm{Re}\{h_3\} \leqslant h_4$ to preserve the ordering). This regime allows for relatively exotic interfacial gravity capillary waves of the type discussed in connection with the modified KdV equation by Laget & Dias (1997, figure 5).

Example plots of generic 'potential functions' $-3P(h)/N(h)$ for nonlinear waves in the low and high surface tension (case I) regimes are illustrated in figure 3(*a*, *b*). A potential function for the high surface tension situation (case II)is shown in figure 3(*h*).

3.2. *Special case I: the linear wave limit*

Results are presented here for the low surface tension case. Except where stated otherwise, identical results emerge for the high surface tension (case I) regime. Taking the limit $h_2, h_3 \to \bar{h}$ allows the wavenumber, k, (3.12) to be evaluated as

$$k = \sqrt{\frac{3(\bar{h} - h_1)(h_4 - \bar{h})}{N(\bar{h})}}. \tag{3.17}$$

The relations (3.10) and (3.11) reduce to the following results for the linear wave speed, c_0, and background shear, $\bar{v}$,

$$c_0 = \bar{h}\sqrt{h_1 h_4} + (1-\bar{h})\sqrt{(1-h_1)(1-h_4)} \quad \text{and} \quad \bar{v} = \sqrt{(1-h_1)(1-h_4)} - \sqrt{h_1 h_4}, \tag{3.18}$$

and these can be used to eliminate h_1 and h_4 from (3.17) in favour of c and $\bar{v}$, yielding the following dispersion relation for the linear phase speed $c = c_0(k)$,

$$\begin{aligned} \left(1 + \tfrac{1}{3}k^2\bar{h}(1-\bar{h})\right) c_0^2 - 2\bar{v}(1-2\bar{h})c_0 \\ + \bar{v}^2\left(1 - 3\bar{h}(1-\bar{h}) + \tfrac{1}{3}k^2\bar{h}^2(1-\bar{h})^2\right) - \bar{h}(1-\bar{h})(1+\tau k^2) = 0. \end{aligned} \tag{3.19}$$

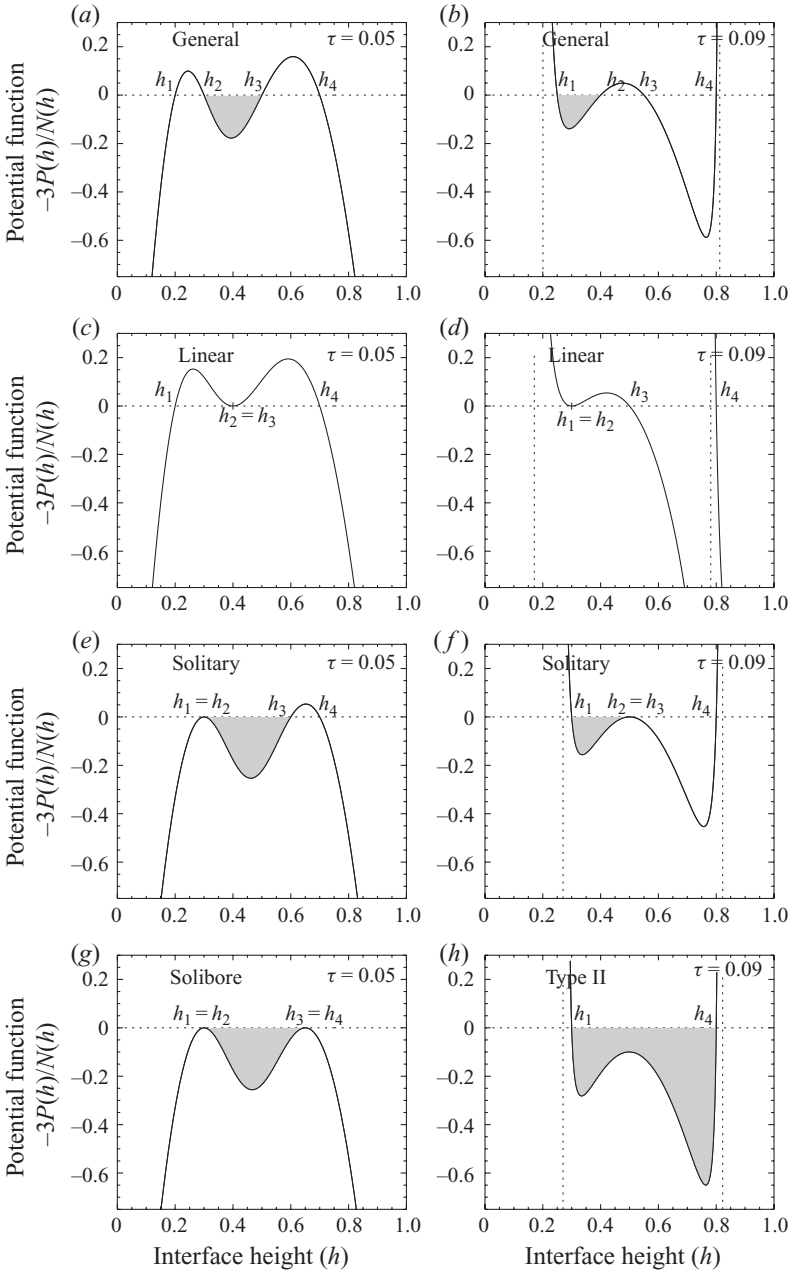

FIGURE 3. Typical structure of the potential function $-3P(h)/N(h)$ in the general, linear and solitary wave cases, corresponding to different values of the constants h_i. Waves of permanent form exist only in potential wells (shaded). (*a,c,e,g*) Low surface tension regime $\tau = 0.05$. (*b,d,f,h*) High surface tension regime $\tau = 0.09$. (*g*) Potential function $-3P(h)/N(h)$ for the case of a solibore (unique to the low surface tension case) and (*h*) the 'Type II' high surface tension situation.

It is straightforward to show that the phase speed $c_0(k)$ given by the roots of (3.19) are real for all k, i.e. the MCC equations are regularised, provided that

$$\tau > \tau_s = \tfrac{1}{3}\bar{v}^2\bar{h}(1-\bar{h}). \tag{3.20}$$

For relatively low values of $\bar{v}$, $\tau_s < \tau_c' = c_0^2/3$, and consequently regular linear waves of all wavenumbers exist in the low surface tension regime for $\tau \in [\tau_s, \tau_c']$. The linear dispersion relation (3.19) can of course be obtained directly by linearisation of the MCC equations (2.5) about a mean state $(\bar{v}, \bar{h})$ following Liska *et al.* (1995). However, the approach adopted above will allow an important point regarding the relationship between the linear and solitary wave dispersion relations to be made explicit below.

It is convenient for the application of El's technique to write (3.19) in terms of the Riemann invariants (2.20)

$$\left(1+\frac{1}{3}k^2H\right)c_0^2-(L+R)c_0+\frac{1}{16}(3L+R)(L+3R)-Hk^2\left(\tau+\frac{1}{48}(R-L)^2-\frac{1}{3}H\right)=0, \tag{3.21}$$

where $H = H(L, R)$ is given by (2.27). The quadratic can be solved to obtain the roots

$$c_0^l = \frac{V^l(L, R) - \mathscr{C}(k^2, L, R)}{1 + k^2H/3}, \qquad c_0^r = \frac{V^r(L, R) + \mathscr{C}(k^2, L, R)}{1 + k^2H/3}, \tag{3.22}$$

where $V^r = (1/4)(3R + L)$ and $V^l = (1/4)(3L + R)$ are the long wave speeds (2.21) and

$$\mathscr{C}(k^2, L, R) = \left(\frac{R-L}{4}\right) \times \left(\left\{1 + \frac{4k^2H}{3(R-L)^2}\left(12\tau - 4H - (L+R)^2 + \frac{(R-L)^2}{2}\right) + \frac{16k^4H^2}{3(R-L)^2}\left(\tau - \frac{H}{3} + \frac{(R-L)^2}{48}\right)\right\}^{1/2} - 1\right). \tag{3.23}$$

Example plots of the potential function $-3P(h)/N(h)$ for both low and high surface tension linear waves are illustrated in figure 3(c, *d*).

3.3. *Special case II: the solitary wave limit*

The solitary wave limit in the low surface tension regime, for solitary waves with positive polarity, is the limit $h_1, h_2 \to \bar{h}$, where $(\bar{v}, \bar{h})$ now refer to the background baroclinic velocity and interface height far from the solitary wave. (Waves of negative polarity, given by $h_3, h_4 \to \bar{h}$, are identical under the up–down symmetry and do not require separate treatment.) Example plots of the potential function $-3P(h)/N(h)$ for both low and high surface tension solitary waves are illustrated in figure 3(*e*,*f*).

Can the solitary wave speeds, c_s, be expressed as a function of the wave amplitude $c_s = c_s(a)$? In the solitary wave limit (3.10) and (3.11) become

$$c_s = \bar{h}\sqrt{h_3h_4} + (1-\bar{h})\sqrt{(1-h_3)(1-h_4)} \quad \text{and} \quad \bar{v} = \sqrt{(1-h_3)(1-h_4)} - \sqrt{h_3h_4}, \tag{3.24}$$

which may be combined to give

$$\left.\begin{aligned} h_3h_4 &= (c_s - \bar{v}(1-\bar{h}))^2 = (c_s - \bar{u}_2)^2, \\ (1-h_3)(1-h_4) &= (c_s + \bar{v}\bar{h})^2 = (c_s - \bar{u}_1)^2, \end{aligned}\right\} \tag{3.25}$$

where $\bar{u}_1$ and $\bar{u}_2$ are the background upper and lower layer velocities. Subtracting the first from the second gives

$$h_3 + h_4 = 1 - 2c_s\bar{v} + \bar{v}^2(1-2\bar{h}), \tag{3.26}$$

which can be used to eliminate h_4 in favour of $h_3 = \bar{h} + a$ in (3.25). A new result, generalising that given in Choi & Camassa (1999, their dimensional formula (3.57) corresponds to the special case with $\bar{v} = 0$), for the solitary wave speed–amplitude relationship is

$$c_s(a) = \bar{v}(1-2\bar{h}-a) \pm \left[(1-\bar{v}^2)(\bar{h}+a)(1-\bar{h}-a)\right]^{1/2}. \tag{3.27}$$

An obvious property of (3.27) is that in the limit $a \to 0$ the two solitary wave speeds c_s^r and c_s^l tend to the long wave speeds V^r and V^l, respectively (2.21). Interestingly, the result is also independent of the surface tension parameter, τ.

An alternative perspective on the solitary wave, useful for the Whitham theory developed below, follows from the definition of the conjugate wavenumber, $\tilde{k}$, where

$$\frac{\pi}{\tilde{k}} = \frac{1}{\sqrt{3}} \int_{h_1}^{h_2} \frac{\sqrt{N(h)}}{\sqrt{-P(h)}} \, \mathrm{d}h, \tag{3.28}$$

in the low surface tension regime. In the solitary wave limit ($k \to 0$), the conjugate wavenumber serves as a parametrisation of the solitary wave amplitude, and below will prove more convenient than the direct use of a itself. Taking $h_1, h_2 \to \bar{h}$ as above gives

$$\tilde{k} = \sqrt{\frac{3(h_4 - \bar{h})(h_3 - \bar{h})}{N(\bar{h})}}, \tag{3.29}$$

and substituting for h_3 and h_4, following the procedure for the linear wave case, the conjugate dispersion relation for $c_s = c_s(\tilde{k})$ is obtained

$$\begin{aligned} \left(1 - \tfrac{1}{3}\tilde{k}^2\bar{h}(1-\bar{h})\right) c_s^2 - 2\bar{v}(1-2\bar{h})c_s \\ + \bar{v}^2\left(1 - 3\bar{h}(1-\bar{h}) - \tfrac{1}{3}\tilde{k}^2\bar{h}^2(1-\bar{h})^2\right) - \bar{h}(1-\bar{h})(1-\tau\tilde{k}^2) = 0. \end{aligned} \tag{3.30}$$

The linear dispersion relation (3.19) is related to the conjugate expression (3.30) via $c_0(k) = c_s(\mathrm{i}k)$, and the Riemann invariant form of the conjugate dispersion relation, which will be useful below, is

$$\begin{aligned} \left(1 - \frac{1}{3}\tilde{k}^2 H\right) c_s^2 - (L+R)c_s + \frac{1}{16}(3L+R)(L+3R) \\ + H\tilde{k}^2\left(\tau + \frac{1}{48}(R-L)^2 - \frac{1}{3}H\right) = 0. \end{aligned} \tag{3.31}$$

3.4. *Special case III: the solibore*

An important solution, which exists only for the low surface tension case (*a*, discussed in § 3.1), is the 'solibore' (Choi & Camassa 1999). A solibore smoothly connects a left state (v_-, h_-) to a right state (v_+, h_+) and is an exact energy-conserving (i.e. non-turbulent) internal hydraulic jump or bore. On long length scales (i.e. in the SWE limit) the solibore appears as a discontinuity, and might be thought to be analogous to the 'weak solutions' (momentum-conserving hydraulic jumps) of the single-layer SWE. However, given a particular direction of propagation, a specified downstream state (v_+, h_+) connects to just a single possible solibore solution with a uniquely defined propagation speed. By contrast, a specified downstream state in the single-layer SWE can be connected to a single-parameter family (a so-called 'Hugoniot loci') of possible upstream states via a weak solution/hydraulic jump. The family of hydraulic jumps is parametrised by the velocity of the hydraulic jump itself.

Here a somewhat different treatment to that of Choi & Camassa (1999) is presented in order to support the results below. The solibore limit is given by $h_1, h_2 \to h_-$, $h_3, h_4 \to h_+$ (see figure 3*g*). The solibore speed $c = c_b$ obtained from (3.10) is, therefore,

$$c_b = \pm(1 - (h_+ + h_-) + 2h_-h_+), \tag{3.32}$$

and (3.11) becomes

$$v_+ = \pm(1 - 2h_-), \qquad v_- = \pm(1 - 2h_+), \tag{3.33}$$

where the positive signs correspond to rightward-travelling waves in each case.

The result above allows an important connection to be made with the underlying two-layer SWE system discussed in § 2. The relation (3.33) is identical to the shear/buoyancy symmetry described in § 2.4. Therefore, solibores connect left and right states with equal long-wave Riemann invariants (L, R), which are conserved under the shear/buoyancy mapping. Hence, the long-wave Riemann invariants are conserved across, but not within, a solibore. In terms of the right state (v_+, h_+) and the Riemann invariants (L, R) the solibore speed is

$$c_b = \tfrac{1}{2} + \tfrac{1}{2}v_+(1 - 2h_+) = \tfrac{1}{2} + \tfrac{1}{4}(L + R). \tag{3.34}$$

4. Dam breaks in the MCC equations

In this section the development of the MCC Gurevich–Pitaevskii problem, i.e. the flow generated from initial conditions (2.6), is considered. First, it will be verified that the MCC system satisfies the conditions necessary for El's technique for 'dispersive shock fitting' to be applied. The reader is referred to El (2005, see also El *et al.* 2005, 2006), where the theory is developed and the necessary conditions are derived. El's technique is then applied to the problem at hand.

4.1. *Applicability of El's technique for 'dispersive shock fitting'*

In order for 'dispersive shocks' or undular bores to be 'fit' into solutions of an underlying non-dispersive set of equations, supporting bidirectional wave propagation, the system of equations must be first amenable to Whitham averaging (following Whitham 1965). The Whitham average can be interpreted as a local 'wavelength average', on the understanding that the envelope of the wavetrain in question is slowly varying in space and time. In the case of the (low surface tension) MCC the Whitham average of any function $F(v, h)$ of baroclinic velocity, v, and interface height, h, can be written as

$$\bar{F} = \frac{k}{2\pi}\int_0^{2\pi/k} F(v, h)\,\mathrm{d}x = \frac{k}{\sqrt{3}\pi}\int_{h_2}^{h_3} \frac{F\,(v(h), h)\,\sqrt{N(h)}}{\sqrt{P(h)}}\,\mathrm{d}h. \tag{4.1}$$

Here k is the wavenumber (3.12) and $v(h)$ is given by (3.11), so it is notable that $\bar{F}$, i.e. the Whitham average of any function of (v, h), can be expressed entirely in terms of the four roots h_i (see (3.5)). The four roots h_i can be considered to be the prognostic variables for the Whitham averaged equations, and for consistency are taken to vary slowly across the modulated wavetrain. The choice of the overbar for the Whitham averaging operator here is deliberate, as it is entirely consistent with its use in the linear and solitary wave limits above. An important property of the Whitham average (4.1) is that $\bar{F} = F(\bar{v}, \bar{h})$ in either the solitary $h_1 \to h_2$ or linear $h_2 \to h_3$ limits (e.g. El 2005).

El (2005) lists several further conditions that the system under investigation must satisfy.

(*a*) The system admits the classical hyperbolic dispersionless limit which is formally obtained by introducing stretched variables ($X = \epsilon x$, $T = \epsilon t$ and taking $\epsilon \to 0$). As discussed above, for the case of the MCC, the dispersionless limit is the two-layer SWE (2.16).

(*b*) The system supports at least three conservation laws. Whitham modulation equations are best derived from conservation laws of the full system (e.g. Kamchatnov 2000), as the Whitham averaging operator commutes with space and time derivatives. Therefore, the three laws can be averaged as

$$\overline{(\mathscr{P}_{it})} + \overline{(\mathscr{Q}_{ix})} = \bar{\mathscr{P}}_{it} + \bar{\mathscr{Q}}_{ix} = 0, \quad i = 1, 2, 3. \tag{4.2}$$

In the case of the MCC the three conservation laws are those given above for mass (2.7), energy (2.8) and irrotationality (2.11). The Whitham modulation equations are completed by the wavenumber conservation law

$$k_t + (ck)_x = 0, \tag{4.3}$$

which corresponds to a consistency condition in the formal asymptotic procedure corresponding to the Whitham averaging, and can be treated as a fourth conservation law (i.e. $\mathscr{P}_4 = k$, $\mathscr{Q}_4 = ck$).

(*c*) The system must support periodic travelling waves parametrised by four independent integrals of motion. For the MCC the waves satisfy (3.5) and the four parameters are, for example, the four roots h_i of $P(h)$. The potential function is required to have at least three real zeros ($-3P(h)/N(h)$ in (3.5) typically has four roots, see figure 3) and must exhibit quadratic behaviour in the linear and solitary wave limits, verified for the MCC under certain restrictions on surface tension τ in §§ 3.2 and 3.3.

(*d*) The Whitham modulation system itself must remain hyperbolic and genuinely nonlinear for the solutions under study. It is not possible to verify these final conditions without direct solution of the Whitham system itself, a contingency which El's technique is designed to circumvent, so this condition can be verified only by an *a posteriori* check on the modulational stability of the undular bore (e.g. by comparison with a numerical solution). As shown in § 2.4, the underlying two-layer SWE are not genuinely nonlinear for generalised lock-exchange flows, and the application of El's technique in this case will be discussed further below.

El's technique determines the leading and trailing edges of the undular bore in two separate calculations. The key step in finding the linear (assumed here to be the trailing) edge involves the integration of the zero wave amplitude ($a \to 0$), reduction of the Whitham system across the undular bore. For the MCC, the $a \to 0$ limit is

$$a = 0 : \begin{cases} \bar{h}_t + (\bar{v}\bar{h}(1-\bar{h}))_x = 0, \quad \bar{v}_t + \left(\frac{1}{2}\bar{v}^2(1-2\bar{h}) + \bar{h}\right)_x = 0, \\ k_t + (kc_0(\bar{v}, \bar{h}, k))_x = 0, \end{cases} \tag{4.4}$$

with c_0 given by the appropriate root of (3.19). The $a \to 0$ reduction is, therefore, the two-layer SWE (2.16) augmented with a linear wavenumber conservation law, and the integral is performed from the downstream state $(v_+, h_+, 0)$ to find the upstream state (v_-, h_-, k_-). A unique solution (for a rightward-travelling undular bore) is determined by imposing the condition that the left Riemann invariant L is conserved across the bore (i.e. $L_- = L_+$). The conservation of L across the bore can be deduced from the time-reversibility property of the MCC (see El 2005, § VB). The wavenumber k_- is the linear wavenumber at the trailing edge of the undular bore, and the speed of the trailing edge is given by the linear group velocity there $s_- = \partial(kc_0)/\partial k\,(k_-, v_-, h_-)$. It is important to emphasise that the above calculation reveals nothing about the internal structure of the undular bore but is useful only in matching the end conditions across it (see the discussion in section IIIE of El 2005).

To find the details of the leading edge an analogous matching calculation must be performed using the zero wavenumber ($k \to 0$) reduction of the Whitham system. It

turns out to be more useful to use the variables $\tilde{k}$ (the conjugate wavenumber given by 3.28) and $\Lambda = k/\tilde{k}$ in place of a and k and to consider the limit $\Lambda \to 0$. The $k \to 0$ wavenumber limit of the Whitham system is then found to consist of the two-layer SWE as in (4.4) augmented by a conjugate wavenumber conservation law

$$\tilde{k}_t + \left(\tilde{k} c_s(\tilde{k}, \bar{v}, \bar{h})\right)_x = 0, \tag{4.5}$$

where here c_s is the solitary wave speed given by the appropriate root of (3.31). The integral is this time from the upstream state $(v_-, h_-, 0)$ to find the downstream state $(v_+, h_+, \tilde{k}_+)$, with $L_- = L_+$ imposed as before. The amplitude of the solitary wave at the leading edge speed is determined by $\tilde{k}_+$ and the speed of the upstream edge is given by the solitary wave speed $s_+ = c_s(\tilde{k}_+, v_+, h_+)$. Finally, a necessary consistency check is that the trailing and leading edge speeds satisfy the appropriate 'entropy' conditions (El 2005)

$$V_-^l < s_- < V_-^r, \quad V_+^r < s_+, \quad s_+ > s_-. \tag{4.6}$$

4.2. *Application of El's technique to Miyata–Camassa–Choi dam-break flows*

It is now established that El's technique can be applied to a typical MCC dam-break flow. The most physically relevant initial conditions (2.6) satisfy $v_- = v_+ = 0$, i.e. the fluid is initially at rest, and $h_+ < h_- < 1/2$. It is straightforward to deduce that a generalised dam break will result, and that it will resolve itself as illustrated in figure 1(*a*,*b*) (see El *et al.* 2006), because as established above the left Riemann invariant L is conserved across a right-travelling simple undular bore and the right Riemann invariant R across a left-travelling rarefaction wave. It follows that the mid-state (v_m, h_m), illustrated in figures 4(*b*) and 4(*d*), has Riemann invariants $(L_m, R_m) = (L_+, R_-)$, where $L_+ = -2\sqrt{h_+(1-h_+)}$ and $R_- = 2\sqrt{h_-(1-h_-)}$. Since the behaviour of the leftwards-travelling rarefaction wave has been considered in § 2.5, we only need to consider the simple undular bore connecting (v_+, h_+) and (v_m, h_m).

To obtain the speed of the 'linear wave' edge of the undular bore the zero-amplitude reduction of the Whitham equations must be integrated across the bore. For definiteness, as above, it will be assumed that the 'linear wave' edge is the trailing edge (where $(L, R) = (L_m, R_m)$), an assumption which will be shown below to be true for low surface tension undular bores. The left Riemann invariant L is conserved across the undular bore, hence the two-layer SWE in (4.4) can be replaced by $R_t + V^r R_x = 0$, and the nature of the characteristic solution requires that the solution of (4.4) must have the form $k = k(R)$. It follows that

$$\frac{\mathrm{d}k}{\mathrm{d}R} = \frac{k\left(\partial c_0^r/\partial R\right)}{V^r - c_0^r - k\left(\partial c_0^r/\partial k\right)} \quad \text{with} \quad k(R_+) = 0, \tag{4.7}$$

where c_0^r is the right propagating solution of (3.21). Implicit differentiation of (3.21) with respect to k and R, followed by some elementary rearrangements, results in

$$\begin{aligned}\frac{\mathrm{d}(k^2)}{\mathrm{d}R} &= \frac{\frac{3}{4}R + \frac{5}{4}L - 2c_0^r + 2k^2\left[H_R\left(\frac{1}{3}\left(c_0^{r\,2} + 2H\right) - \tau - \frac{1}{48}(R-L)^2\right) - \frac{1}{24}H(R-L)\right]}{k^{-2}\left(V^r - c_0^r\right)\left(R + L - 2\left(1 + \frac{1}{3}k^2 H\right)c_0^r\right) - 2H\left(\frac{1}{3}\left(c_0^{r\,2} + H\right) - \tau - \frac{1}{48}(R-L)^2\right)}, \\ &= \frac{3(R-L)}{2H(2H + R(R+L) - 6\tau)}, \quad \text{when } k = 0,\end{aligned} \tag{4.8}$$

where $H = H(L, R)$ is given by (2.27) and $H_R \equiv \partial H/\partial R$. The lower expression is necessary to evaluate $\mathrm{d}(k^2)/\mathrm{d}R$ when $k = 0$, and is obtained from the upper expression

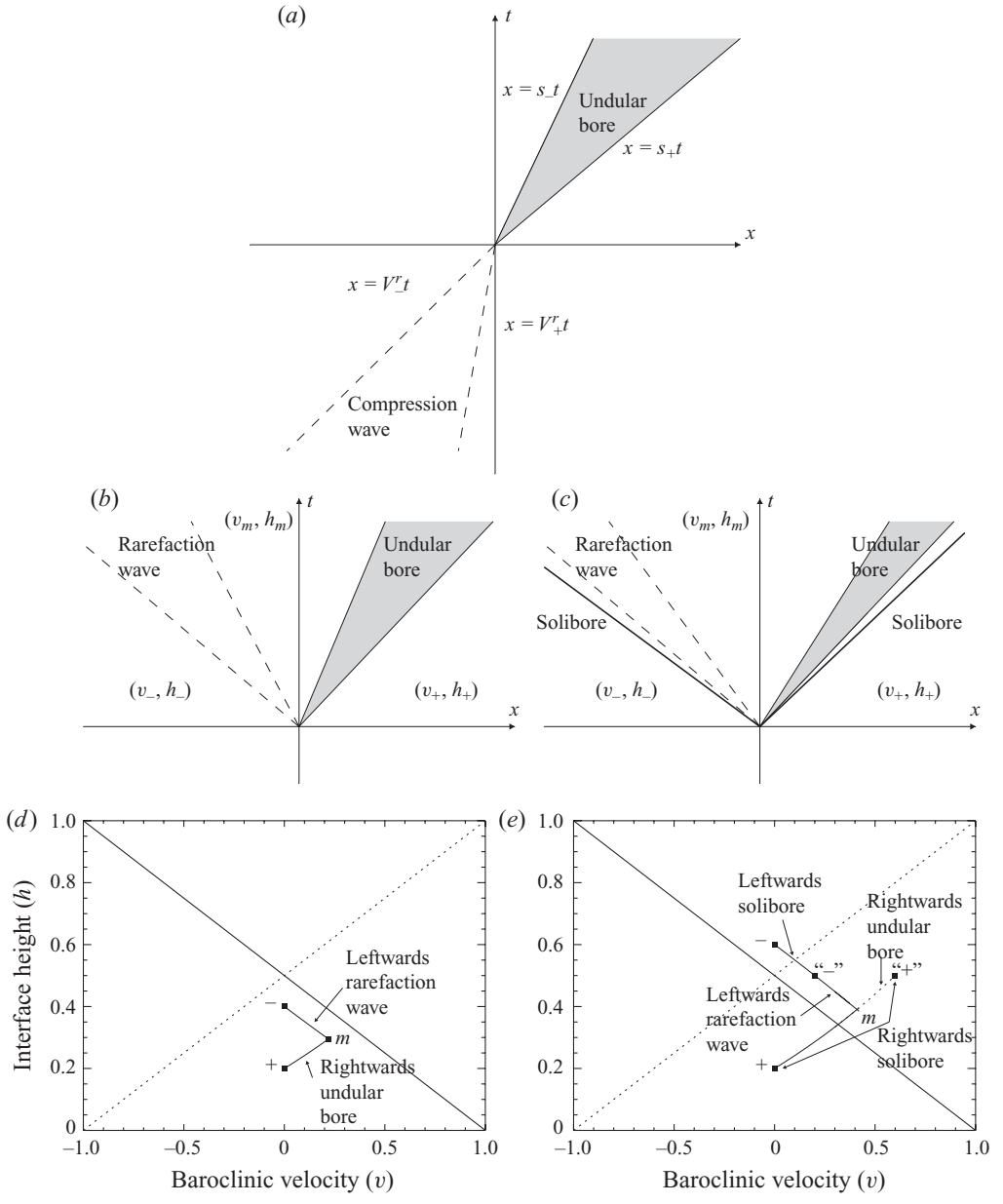

FIGURE 4. (*a*) Development in the (x, t) plane of a simple rightward-propagating undular bore. Time reversibility in the MCC system implies that such a solution can be continued into $t < 0$, where the solution is a two-layer SWE simple wave of compression. (*b*) The typical development in the (x, t) plane of 'dam-break' initial conditions ($v_- = v_+ = 0$, $h_+ < h_- < 1/2$). (*c*) The typical development in the (x, t)-plane of 'lock-exchange' initial conditions ($v_- = v_+ = 0$, $h_+ < 1/2 < h_-$). (*d*) A (v, h) diagram illustrating how the resolved states are connected for the dam break initial conditions. (*e*) As (*d*), but for the lock-exchange initial conditions.

from the limit

$$\lim_{k\to 0} k^{-2}(V^r - c_0^r) = \frac{H(2H + R(R+L) - 6\tau)}{3(R-L)}. \tag{4.9}$$

A prediction for the wavenumber at the trailing edge of the undular bore $k(R_-)$ is obtained by integrating the ordinary differential equation (ODE, (4.8)) forwards over the interval $[R_+, R_-]$ ($R_- > R_+$), with the boundary condition $k(R_+) = 0$. In the single-layer case, the corresponding ODE can be integrated analytically (El *et al.* 2006), but here it appears we are restricted to numerical solution. The standard fourth-order Runge–Kutta method is used. The trailing edge speed s_- is obtained then from the solution $k(R_-)$, using the expression for the group speed $s_- = \partial(kc_0)/\partial k$ evaluated at $(k, L, R) = (k(R_-), L, R_-)$.

The solitary wave leading edge speed is obtained by closely following the arguments for the linear wave edge, except this time with the zero wavenumber reduction of the Whitham system detailed above. Using the ansatz $\tilde{k} = \tilde{k}(R)$ in (4.5) results in

$$\frac{\mathrm{d}\tilde{k}}{\mathrm{d}R} = \frac{\tilde{k}(\partial c_s^r/\partial R)}{V^r - c_s^r - \tilde{k}(\partial c_s^r/\partial \tilde{k})} \quad \text{with} \quad \tilde{k}(R_-) = 0, \tag{4.10}$$

which can be written explicitly after implicit differentiation of (3.31) as,

$$\begin{aligned}\frac{\mathrm{d}(\tilde{k}^2)}{\mathrm{d}R} &= \frac{\frac{3}{4}R + \frac{5}{4}L - 2c_s^r - 2\tilde{k}^2\left[H_R\left(\frac{1}{3}\left(c_s^{r\,2} + 2H\right) - \tau - \frac{1}{48}(R-L)^2\right) - \frac{1}{24}H(R-L)\right]}{\tilde{k}^{-2}\left(V^r - c_s^r\right)\left(R + L - 2\left(1 - \frac{1}{3}\tilde{k}^2 H\right)c_s^r\right) + 2H\left(\frac{1}{3}\left(c_s^{r\,2} + H\right) - \tau - \frac{1}{48}(L-R)^2\right)}. \\ &= -\frac{3(R-L)}{2H(2H + R(R+L) - 6\tau)} \quad \text{when } \tilde{k} = 0, \end{aligned} \tag{4.11}$$

where c_s^r is the greater root of (3.31) corresponding to the rightward-propagating solitary wave. The ODE (4.11) can be integrated backwards in R over the interval $[R_+, R_-]$, starting from the boundary condition $\tilde{k}(R_-) = 0$, to obtain the leading edge conjugate wavenumber $\tilde{k}(R_+)$. The leading edge speed of the undular bore is then given by $s_+ = c_s^r(\tilde{k}(R_+), L, R_+)$, and the amplitude, a, of the leading edge solitary wave can then be obtained by numerical solution of (3.27) to obtain a from $c_s(a)$.

Figure 5(a, c, e) shows snapshots of the development of a simple undular bore in the low surface tension regime ($\tau = 0.05$) calculated numerically (see Appendix A for details). The initial conditions are $(v_+, h_+) = (0, 0.25)$ and $(v_-, h_-) = (0.1388, 0.3125)$, and the initial slope is smoothed with a tanh-profile of half-width 2 (scaled on the channel depth H). The vertical dotted lines denote the predicted locations of the leading and trailing edges, and the horizontal line the solitary wave amplitude prediction, derived from the results above. It is clear that the theoretical predictions from El's technique are reasonably accurate for this example. Figure 5(b, d, f) shows snapshots of the development of a rightward-propagating rarefaction wave generated if the initial conditions are reversed, i.e. $(v_+, h_+) = (0.1388, 0.3125)$ and $(v_-, h_-) = (0, 0.25)$. In this case the dotted lines are predictions based on two-layer SWE rarefaction waves (see § 2.5). A straightforward calculation reveals that the entropy conditions (4.6) are satisfied for the case of this low surface tension undular bore. At higher surface tensions the entropy conditions fail for this undular bore, and there is a quite distinct behaviour, as discussed in Appendix B.

Theoretical predictions have been tested further using a range of numerical simulations. The results are presented in figure 6. Fixing $(v_+, h_+) = (0, 0.25)$ (so that $L_+ = -\sqrt{3}/2$ $R_+ = \sqrt{3}/2$) for each experiment, the right-step height h_- has been varied in the range [0.25, 0.325], with corresponding adjustments in v_- to maintain the simple undular bore transition condition $L_- = L_+$. A comparison between theoretical (solid curves) and numerical calculations (points, see Appendix A for details) of the undular bore edge positions reveals good agreement up to $h_- = 0.3$, with increasingly poor agreement afterwards. The theoretical calculations are in fact halted where turning

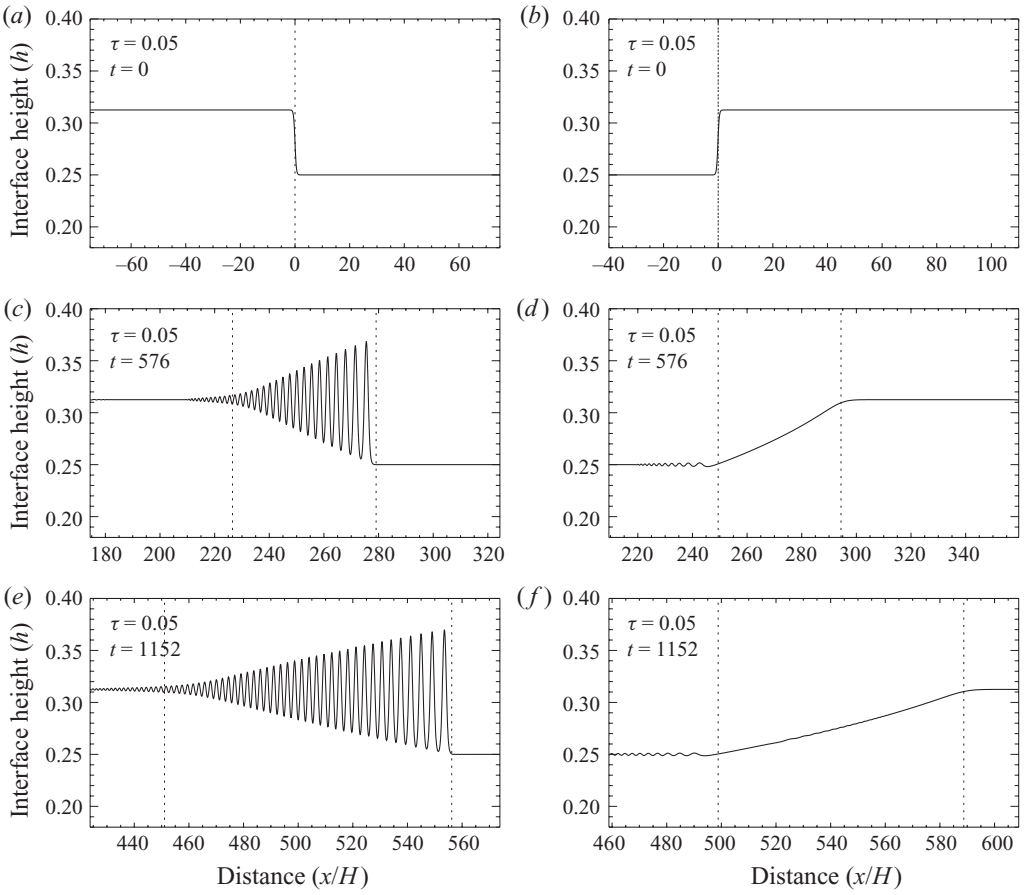

FIGURE 5. (*a,c,e*) Snapshots of interface height from a numerical simulation of a rightward-propagating undular bore with initial conditions $L_- = L_+ = -\sqrt{3}/2$, $R_+ = \sqrt{3}/2$, $R_- = 0.9701$ and with low surface tension ($\tau = 0.05$). Dotted lines show the theoretical predictions of the locations of the leading solitary wave edge and trailing linear wave edge. (*b,d,f*) Snapshots of a rightward-propagating rarefaction wave developed from 'mirror image' initial $L_- = L_+ = -\sqrt{3}/2$, $R_+ = 0.9701$, $R_- = \sqrt{3}/2$, also for low surface tension ($\tau = 0.05$).

points in s_+ and s_- are detected, as turning points generally indicate breakdown in the original assumptions for the structure of the undular bore, suggesting that partial undular bores (El *et al.* 2006), which are characterised by a rapid spatial transition at the trailing edge from finite amplitude waves to an undisturbed flow, will be formed.

The dotted curves show the predictions that follow from approximating weakly nonlinear long wave (KdV) limit, obtained from Taylor expansions of (4.8) and (4.11) for $(R_- - R_+)$, k^2, $\tilde{k}^2 \ll 1$ and retaining only up to quadratic terms in k, $\tilde{k}$ in the Taylor expansions of (3.21) and (3.31). The results for the trailing and leading edge velocities are

$$s_- = V_+^r - \tfrac{3}{4}(R_- - R_+), \quad s_+ = V_+^r + \tfrac{1}{2}(R_- - R_+), \quad \text{(linear/solitary)} \tag{4.12}$$

and are similar to results for the single-layer case presented in El *et al.* (2006, equations (52) and (53)). Interestingly, surface tension drops out of the weakly nonlinear

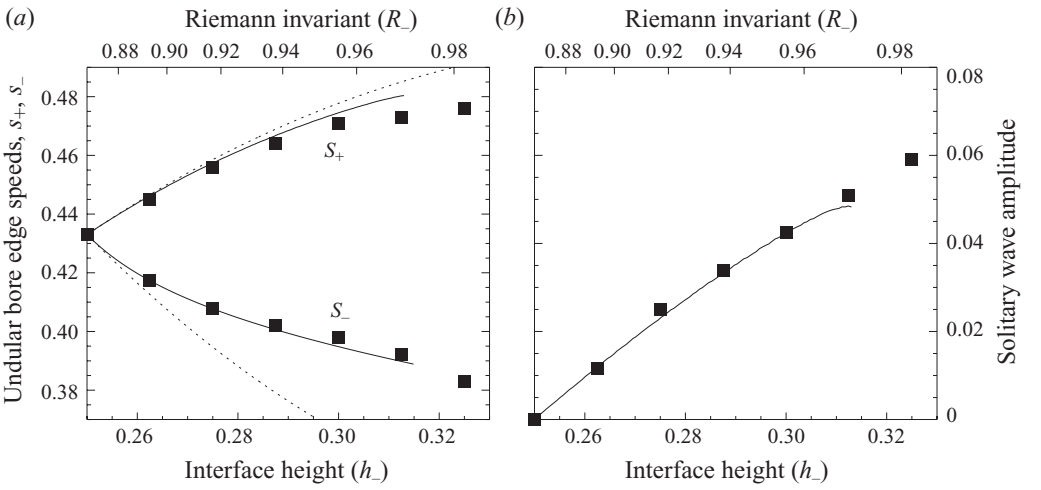

FIGURE 6. (*a*) Predictions using Whitham theory (solid curves) and its weakly nonlinear approximation (dotted curves, see (4.12)) for the solitary edge speed s_+ and linear edge speed s_- compared with the low surface tension ($\tau = 0.05$) set of numerical simulations (points). Initial conditions are given by $L_- = L_+ = -\sqrt{3}/2$, $R_+ = \sqrt{3}/2$, $R_- \in [0.866, 1]$. (*b*) Predictions of lead solitary wave amplitude versus numerical results for the $\tau = 0.05$ set.

predictions of s_- and s_+ entirely, except for an interesting 'switch in polarity' effect that occurs as a critical value of $\tau = \tau_c$ is crossed, discussed in Appendix B below.

4.3. *Application of El's technique to Miyata–Camassa–Choi lock-exchange flows*

The dam-break flows described above exhibit broadly similar behaviour to the corresponding single-layer flows (El *et al.* 2006). What about lock-exchange flows? Concentrating on the 'fluid at rest' initial conditions with $h_+ < 1/2 < h_-$ and $v_+ = v_- = 0$, and following the same arguments as above, rightward- and leftward-travelling waves will be connected to a mid-state (v_m, h_m) defined by $(L_m, R_m) = (L_+, R_-)$. Unlike the dam-break case, however, (v_m, h_m) will be in the shear-dominated quadrant of the (v, h) plane, meaning that both leftward- and rightward-travelling waves are generalised lock-exchange flows according to the definition given in § 2.4.

For the low surface tension regime, in which the solibore is present, there exist simple solutions which satisfy the entropy conditions for both the leftward- and rightward-generalised lock-exchange flows. A schematic illustration is presented in figure 1(*c*,*d*). The basic anatomy of the solutions is given by the constructions in figures 4(*c*) and (*e*), illustrating their development on the (x, t) plane, as well as how the intermediate states are connected on a (v, h) diagram. The leftward- and rightward-travelling solutions consist of a solibore followed by either a rarefaction wave or an undular bore, respectively. The undular bore differs from those generated in generalised dam breaks as it connects left and right states within the shear-dominated (rather than the buoyancy-dominated) regime of the two-layer SWE. The polarity of the solitary waves in the undular bore is, therefore, opposite to those observed in a generalised dam break. The solibore is the fastest propagating (linear or solitary) wave that can propagate into the undisturbed left and right states, and there exists a discrete gap in the (x, t) plane between the propagating solibore and the following undular bore/rarefaction wave. The flow within the gap region is

determined by the 'image' state of the upstream state under the St. Andrew's cross mapping (2.22), marked as '−' and '+' in figure 4(*e*). The undular bore and rarefaction waves that follow each solibore then connect the mid-state (v_m, h_m) to the respective image states.

Numerical solutions of the MCC are required to verify that the above solutions are indeed selected during MCC lock exchanges. A series of simulations of rightward-propagating generalised lock exchange, with the left Riemann invariant held constant across the step in each case ($L_- = L_+$), have been performed, the following four qualitatively different possibilities exist.

(i) The left state is shear dominated (SD) and the right state is buoyancy dominated (BD), with $R_- > R_+$.

(ii) Left state SD, right state BD, $R_- < R_+$.

(iii) Left state BD, right state SD, $R_- > R_+$.

(iv) Left state BD, right state SD, $R_- < R_+$.

Figure 7 shows snapshots of the interface height during numerical simulations of flows corresponding to types I to IV. Dotted lines show the predicted positions of the solibore as well as the leading and trailing edges of the undular bore/rarefaction wave. Lock exchanges of types I and II, which both feature the solibore propagating into an undisturbed 'buoyancy-dominated' state, are those which emerge naturally in the physical lock-exchange problem with no initial flow and $h_+ < 1/2 < h_-$, as illustrated schematically in figure 1. Types III and IV are likely to be relevant to flows over topography with a 'shear-dominated' upstream flow.

It is notable that it takes significantly longer for the long-time asymptotic structure of a generalised lock-exchange flow to emerge, compared with that of a generalised dam-break flow. This can be explained because long wave speeds have a relatively weak dependence on interface height near the relevant diagonal of the St Andrew's cross. Differences in wave speeds within a generalised lock-exchange flow are, therefore, typically smaller than within a dam-break flow with the same initial interface jump. Finally, it is noteworthy that the MCC equations predict the existence of a 'perfect' lock exchange for $h_- = 1 - h_+$, in which the initial interface jump separates exactly into a leftward- and rightward-propagating solibore.

5. Summary and conclusions

'Dispersive' dam break and lock-exchange initial-value problems have been considered in a Boussinesq two-layer fluid. The results are applicable to the physical situation, where the height difference across the barrier is sufficiently small, and the barrier release sufficiently smooth, to prevent significant wave breaking and to allow an undular bore to develop. The analysis is, therefore, complementary to that of 'strong' dam-break problems, including gravity currents, which require an explicit model of wave-breaking behaviour at a turbulent bore. For the dispersive problem, an appropriate model is the Miyata–Choi–Camassa equations, which do not permit wave breaking but capture leading-order dispersive effects in the presence of strong nonlinearities. It has been demonstrated that the long-time asymptotic behaviour of solutions of the MCC can be deduced using a technique due to El (2005, see also references therein), based on Whitham modulation theory, which allows undular bores to be 'fit' into solutions of the underlying long wave equations of a certain class of regularised nonlinear hyperbolic systems supporting bidirectional wave propagation.

By considering the long wave (two-layer SWE) limit, a formal distinction has been made between generalised dam-break and generalised lock-exchange flows, based on

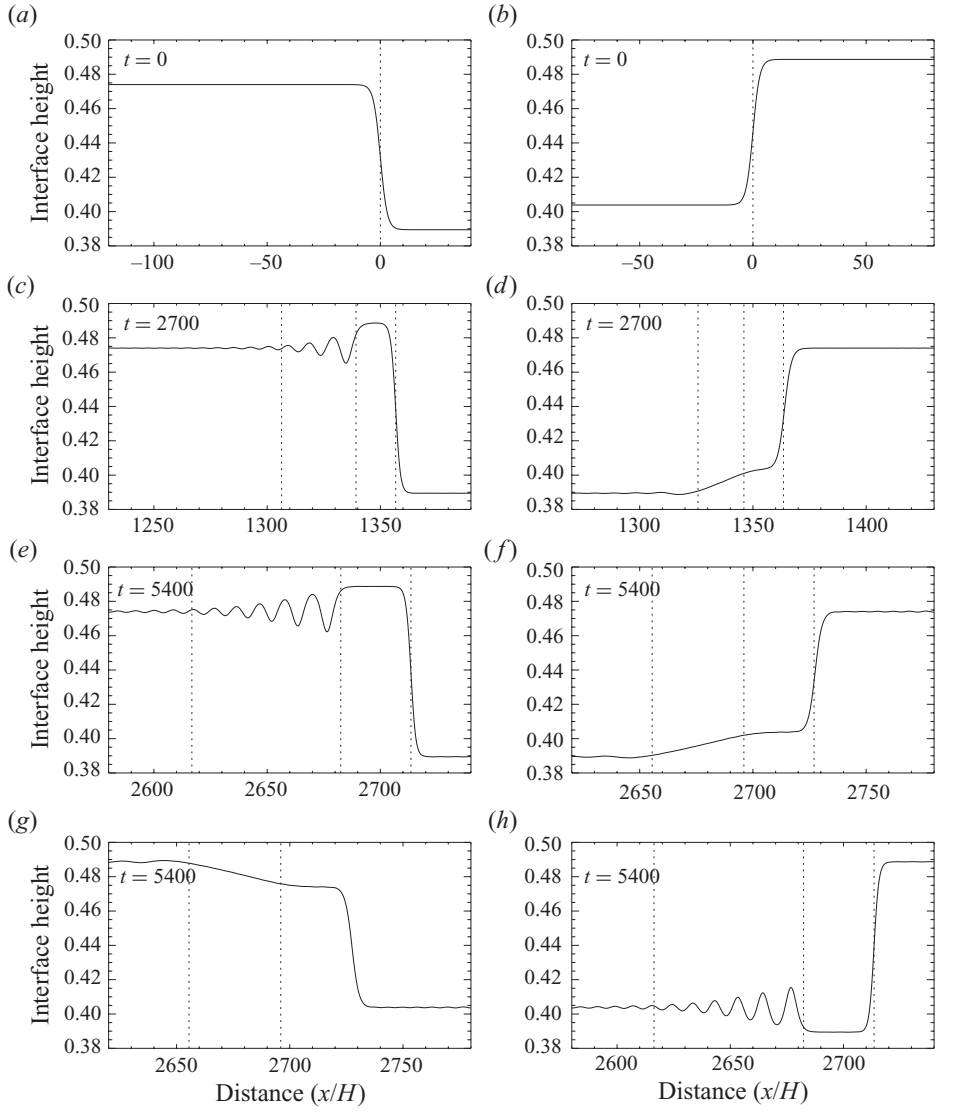

FIGURE 7. Snapshots of numerical simulations of the four types of generalised lock exchanges with low surface tension ($\tau = 0.05$) (see text). Dotted lines show the theoretical predictions of the locations of the solibore, and the leading edge and trailing edge speeds of the undular bore/rarefaction waves. (*a,c,e*) Type I, initial conditions $L_- = L_+ = -0.97$, $R_- = 0.99$ (shear dominated), $R_+ = 0.98$ (buoyancy dominated). (*g*) Type II, $L_- = L_+ = -0.97$, $R_- = 0.98$ (SD), $R_+ = 0.99$ (BD). (*b,d,f*) Type IV, $L_- = L_+ = -0.97$, $R_- = 0.98$ (BD), $R_+ = 0.99$ (SD). (*h*) Type III, $L_- = L_+ = -0.97$, $R_- = 0.99$ (BD), $R_+ = 0.98$ (SD).

the 'St Andrew's cross' mapping between the two-layer and single-layer shallow water equations. Generalised dam breaks must have boundary states located within a single quadrant of the (v, h) domain, and depending on which quadrant can be classified as being 'buoyancy dominated' or 'shear dominated'. Unsurprising, given that the MCC equations reduce to the single-layer (Su–Gardner) equations as a wall is approached, buoyancy-dominated dam breaks are found to be closely analogous to dispersive dam breaks in a single-layer fluid (El *et al.* 2006). Shear-dominated dam breaks do not

exhibit radically different behaviour. The MCC model correctly captures sensitivity to increasing surface tension effects, with a reversal in the polarity of solitary waves, and hence the structure of undular bores once the inverse Bond number τ exceeds a critical value τ_c. A rich variety of behaviours is to be expected for $\tau \approx \tau_c$, which merit further investigation.

Generalised lock-exchange flows can be defined as those with boundary states within different quadrants of the 'St Andrew's cross' map. Perhaps surprisingly, at low surface tensions, causally correct solutions of the lock-exchange initial-value problem can be constructed by straightforwardly combining an undular bore or rarefaction wave with a 'solibore' solution of the MCC equations. It has been verified numerically that these solutions do indeed emerge from the initial-value problem, although compared with dam-break solutions they require a relatively long time to emerge from the initial data. Interestingly 'solibore'-like internal waves are regularly observed in shallow seas and coastal oceans (e.g. MacKinnon & Gregg 2003; Hosegood & van Haren 2004), and are often associated with the internal tide.

There are a number of practical obstacles to observing flows described by the solutions above in an experimental setting. The main consideration is probably the long aspect ratio of the channel required, although there may in addition be initialisation issues relating to the barrier release. Nevertheless, we expect the above solutions to be of practical use in the interpretation of internal wave measurements in the ocean and in understanding two-layer flows over topography where wave breaking is not initiated, among other problems of oceanographic importance.

Appendix A. Description of the numerical scheme

Here a brief description of the pseudo-spectral scheme used to solve the MCC equations (2.5) is discussed. Full details are given in Pearce (2009). Solutions are obtained on a periodic domain of length $L = 400$ (where the dimensional unit is the depth H), and a resolution $N = 2048$ Fourier modes is used, corresponding to a grid-resolution $\delta x \approx 0.1$. The initial conditions (2.6) are smoothed by a tanh profile of half-width 2, and to enforce periodicity a second 'mirror-image' step is introduced at $x = L/2$. The dependent variables v and h are then expanded as

$$h(x,t) = \langle h \rangle + \sum_{m=1}^{N} \hat{h}_m(t) \mathrm{e}^{2\pi \mathrm{i} m x/L}, \quad v(x,t) = \sum_{m=0}^{N} \hat{v}_m(t) \mathrm{e}^{2\pi \mathrm{i} m x/L}, \tag{A 1}$$

where $\langle h \rangle = (1/2)(h_- + h_+)$ is the mean depth. Inserting the truncated expansion (A 1) into (2.5) the resulting equations can be written as

$$\left.\begin{aligned} \left(1 + k^2 \frac{\langle h \rangle (1 - \langle h \rangle)}{3}\right) \frac{\mathrm{d}\hat{v}_m}{\mathrm{d}t} &= -\mathrm{i}k \left(1 + \tau k^2\right) \hat{h}_m + \mathrm{i}k \widehat{\mathscr{N}^v}_m + \widehat{\mathscr{N}^{v*}}_m, \\ \frac{\mathrm{d}\hat{h}_m}{\mathrm{d}t} &= -\mathrm{i}k \langle h \rangle (1 - \langle h \rangle) \hat{v}_m - \mathrm{i}k \widehat{\mathscr{N}^h}_m, \end{aligned}\right\} \tag{A 2}$$

where $k = 2\pi m/L$ is the wavenumber of each mode, and

$$\mathscr{N}^v = -\tfrac{1}{2} v^2 (1 - 2h) + \tfrac{1}{3} h^2 \mathscr{G}[v(1-h)] - \tfrac{1}{3}(1-h)^2 \mathscr{G}[-vh] - \tfrac{1}{3} \langle h \rangle (1 - \langle h \rangle) v_{xt}, \tag{A 3}$$

$$\mathscr{N}^{v*} = -\tfrac{1}{3} h_x \left(h \mathscr{G}[-vh] + (1-h) \mathscr{G}[v(1-h)]\right), \tag{A 4}$$

$$\mathscr{N}^h = v(h - \langle h \rangle)(1 - h - \langle h \rangle), \tag{A 5}$$

are the nonlinear and remainder terms to be calculated in real space. The important point is that the dispersive terms involving v_{xxt} appearing in the right-hand side

of (2.5) have been linearised about $\langle h\rangle$ and the linear part subtracted from both sides. Consequently, the solution to the explicit linear part of (A 2) are linear waves satisfying (3.19) for the special case of no background flow $\bar{v}=0$.

The inherent difficulty in time-stepping (A 2) is that both $\mathscr{N}^v$ and $\mathscr{N}^{v*}$ contain nonlinear terms with mixed time and space derivatives. This difficulty is overcome by utilising a multi-step time-stepping scheme in conjunction with an inner iteration which is applied simultaneously to all wavenumbers in spectral space. For the leapfrog scheme with time-step δt, the update formula is

$$\hat{v}_m^{(n+1)} = \hat{v}_m^{(n-1)} + 2\delta t \mathscr{F}_m^{(n)}, \quad \text{where } \mathscr{F}_m^{(n)} = \frac{\left(-\mathrm{i}k(1+\tau k^2)\hat{h}_m + \mathrm{i}k\widehat{\mathscr{N}^v}_m + \widehat{\mathscr{N}^{v*}}_m\right)^{(n)}}{1+(1/3)k^2\langle h\rangle(1-\langle h\rangle)}, \tag{A 6}$$

where the superscript (n) refers to the nth time level $t=t_n=n\delta t$. Next we introduce the baroclinic velocity tendency at the nth time level

$$\mathscr{D}_m^{(n)} = \frac{\hat{v}_m^{(n+1)} - \hat{v}_m^{(n-1)}}{2\delta t}. \tag{A 7}$$

Because the nonlinear terms $\mathscr{N}^v$ and $\mathscr{N}^{v*}$ include time derivatives the update formula at any given time level can be regarded as a system of nonlinear equations in the $\mathscr{D}_m^{(n)}$,

$$\mathscr{D}_m^{(n)} = \mathscr{F}_m^{(n)}\left(\boldsymbol{d}^{(n)}\right), \tag{A 8}$$

where $\boldsymbol{d}^{(n)}$ is the vector with components $\mathscr{D}_m^{(n)}$, $m=0,\ldots,N$. Equation (A 8) must be solved iteratively at each time step before the baroclinic velocity equation can be updated.

The following iterative scheme is used to solve (A 8). Denoting the jth guess for at time level n by the superscript (j,n), a damped iteration is used to obtain converged updates for $\mathscr{D}_m^{(n)}$, with each iteration being applied to all spectral coefficients (values of m) simultaneously

$$\mathscr{D}_m^{(0,n)} = \frac{2\left(\hat{v}_m^{(n)} - \hat{v}_m^{(n-1)}\right)}{\delta t} - \mathscr{D}_m^{(n-1)}, \tag{A 9}$$

$$\mathscr{D}_m^{(j+1,n)} = \gamma\mathscr{F}_m^{(n)}\left(\boldsymbol{d}^{(j,n)}\right) + (1-\gamma)\mathscr{D}_m^{(j,n)}, \quad j\geqslant 0. \tag{A 10}$$

The first guess $\mathscr{D}_m^{(0,n)}$ exploits the multi-step method by making an extrapolation based on the known time tendencies at earlier time levels. The parameter γ controls the relaxation rate of the iteration. The optimal value of γ is found to depend on the maximum interface slope and is generally in the range [0.2, 1]. The iteration is continued until the convergence criterion

$$\frac{\mathrm{Max}_m\left|\mathscr{D}_m^{(j,n)} - \mathscr{F}_m^{(n)}\left(\boldsymbol{d}^{(j,n)}\right)\right|}{\mathrm{Max}_m|\mathscr{D}_m^{(j,n)}|} < \delta_c. \tag{A 11}$$

is satisfied, with the numerical parameter $\delta_c = 10^{-10}$. Generally 5–10 iterations were required for convergence of the moderate wave slopes investigated above.

The model code was tested by comparing solitary wave and solibore speeds against those calculated analytically following the procedures described in § 3. At the stated resolution, accuracy to six significant figures was obtained, for example waves which were substantially steeper than those emerging from the dam-break flows reported above (Pearce 2009), and the accuracy was found to improve further as the wave slope was decreased.

Appendix B. Behaviour of high surface tension dam breaks

Here dam breaks at high surface tension are considered briefly. The high surface tension case is a mathematical curiosity, owing to the reversal in the polarity of solitary waves reported in § 3, which leads to different behaviours to the low surface tension case. Physically, high surface tension is not relevant to the oceanographic application discussed above, but may nevertheless be realisable experimentally using two immiscible fluids.

The breakdown of the theory presented in § 4.2 occurs, by the inspection of (4.8) and (4.11) in the $k, \tilde{k} \to 0$ limits, when τ increases beyond the critical value

$$\tau_c(L, R) = \tfrac{1}{3}H(L, R) + \tfrac{1}{6}R(R + L). \tag{B 1}$$

The value $\tau = \tau_c$ is the weakly nonlinear critical Bond number, defined as the criterion for a switch in polarity of solitary waves in the KdV limit, i.e. the condition for switching between the high and low surface tension regimes. Considering the more general results of § 3 in the weakly nonlinear long wave limit ($c \to V^r$), it is found that $\tau_c = \tau_c'$, as defined by (3.14), only for the case of a stationary background ($\bar{v} = 0$). For $\bar{v} \neq 0$, it is easily shown $\tau_c \geqslant \tau_c'$, as must be the case since it was shown in § 3 that $\tau < \tau_c'$ is a sufficient condition for the existence of waves in the low surface tension regime. An upper bound can also be found to be $\tau_c \leqslant \tau_c' + 1/12$.

For flows in the high surface tension regime with $\tau > \tau_c$, it is clear that the ODEs (4.8) and (4.11) do not give real solutions near $R = R_+$ and $R = R_-$, respectively, under the assumption of a solitary wave leading edge/linear wave trailing edge used above. Under the opposite assumption of a linear wave leading edge/solitary wave trailing edge, however, (4.8) and (4.11) do give real solutions near $R = R_-$ and $R = R_+$ when the direction of integration of each equation is reversed. Solutions constructed from the second assumption can be shown to satisfy the entropy conditions (4.6) for the high surface tension flows. Hence, a reversal in the structure of the undular bore is predicted as τ is increased past τ_c. There remains a possibility of the absence of complete solutions of one or both of (4.8) and (4.11) for values very close to τ_c, corresponding to more exotic behaviours not captured by El's technique (see e.g. the discussion of the fifth-order KdV equation in Laget & Dias 1997, Section 3.4.3). A snapshot of a high surface tension undular bore (for $\tau = 0.09 > \tau_c = 0.0625$ based on the right state (v_+, h_+)) is illustrated in figure 8(a) for identical initial conditions to the $\tau = 0.05$ case shown in figure 5. The theoretical predictions for the leading and trailing edge positions are seen to be well captured. Figure 8(b) shows a snapshot of the corresponding rarefaction wave, which appears almost identical to the corresponding $\tau = 0.05$ rarefaction wave, confirming that surface tension effects are weak outside the undular bore regions. Figure 8(c, d) shows the high surface tension predictions for a set of experiments corresponding to those discussed in connection with figure 6. Similarly good predictions are obtained for the trailing solitary wave edge and leading linear wave edge, which in the weakly nonlinear limit can be shown to be (c.f. (4.12))

$$s_- = V_+^r + \tfrac{1}{4}(R_- - R_+), \quad s_+ = V_+^r + \tfrac{3}{2}(R_- - R_+), \quad \text{(solitary/linear)}. \tag{B 2}$$

Just as for the low surface tension case, τ drops out of the weakly nonlinear limit, but owing to the switch in polarity of the solitary waves the result is nevertheless quite different to (4.12).

Some calculations of high surface tension lock exchanges have also been performed. These exhibit a markedly different behaviour to the low surface tension case, and

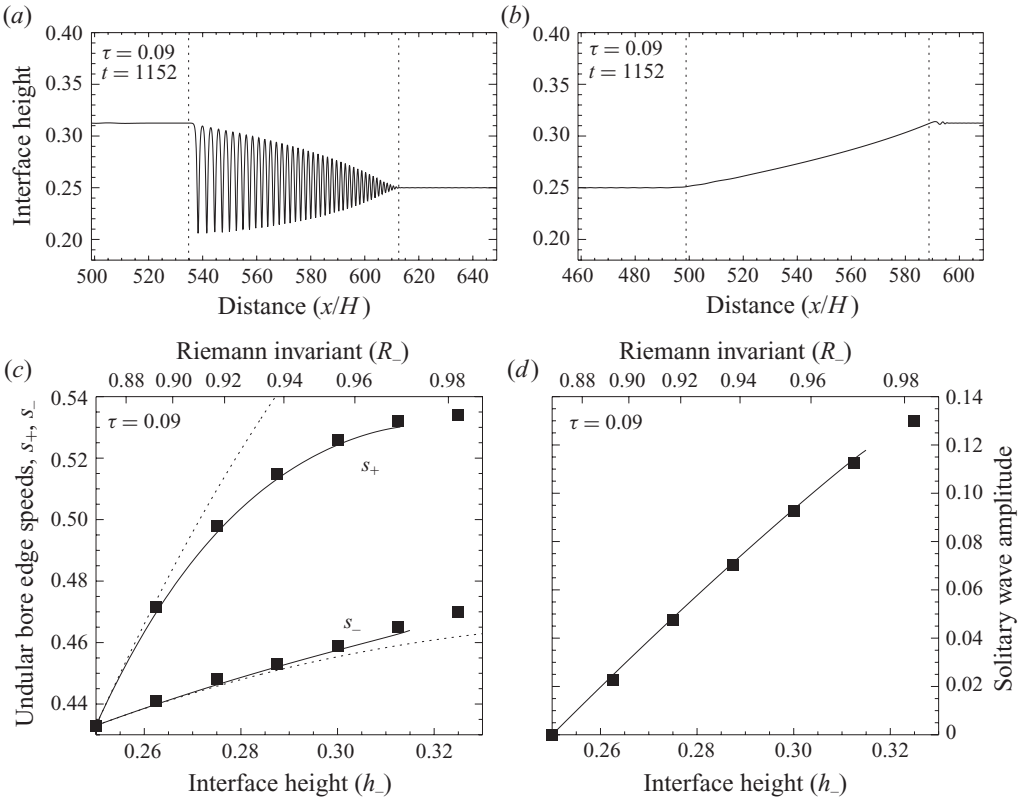

FIGURE 8. (a,b) Snapshots of interface height at $t=1152$ illustrating the development of an undular bore (a) and rarefaction wave (b). Experimental parameters are as for figure 5, but with $\tau=0.09$ (high surface tension regime). Dotted lines show the Whitham theory predictions. (c,d) The Whitham theory predictions (solid lines) versus experimental results (squares) across a suite of experiments, as in figure 6, but for $\tau=0.09$.

merit further study, arguably in the framework of the mathematically somewhat more straightforward, but less realistic, weakly nonlinear context of the extended Korteweg–de Vries equation (following e.g. Grimshaw *et al.* 2002). The solibore does not exist at high surface tension, and solutions consist of dispersive 'compound waves' in which a rarefaction wave and undular bore are seen to merge seamlessly. There may be a useful analogy with the dissipative compound waves featured in hyperbolic systems with non-convex flux functions.

REFERENCES

BAINES, P. G. 1984 A unified description of two-layer flow over topography. *J. Fluid Mech.* **146**, 127–167.

BAINES, P. G. 1995 *Topographic Effects in Stratified Flows*. Cambridge University Press.

BENJAMIN, T. B. 1968 Gravity currents and related phenomena. *J. Fluid Mech.* **31**, 209–248.

BENJAMIN, T. B. & LIGHTHILL, M. J. 1954 On cnoidal waves and bores. *Proc. R. Soc. Lond.* A **224**, 448–460.

BUCKLEY, S. E. & LEVERETT, M. C. 1942 Mechanism of fluid displacements in sands. *Trans. AIME* **141**, 107–116.

CAVANIE, A. G. 1969 Sur la genese et la propagation d'ondes internes dans un millieu a deux couches. *Cahiers Océanographiques* **XXI** (9), 831–843.

Choi, W., Barros, R. & Jo, T.-C. 2009 A regularized model for strongly nonlinear internal solitary waves. *J. Fluid Mech.* **629**, 73–85.

Choi, W. & Camassa, R. 1999 Fully nonlinear internal waves in a two-fluid system. *J. Fluid Mech.* **396**, 1–36.

Chu, V. H. & Baddour, R. E. 1977 Surges, waves and mixing in two-layer density stratified flow. *Proc. 17th Congr. Intl Assoc. Hydraul. Res.* **1**, 303–310.

Chumakova, L., Menzaque, F. E., Milewski, P. A., Rosales, R. R., Tabak, E. G. & Turner, C. V. 2009 Stability properties and nonlinear mappings of two and three layer stratified flows. *Stud. Appl. Maths* **122**, 123–137.

Clarke, J. C. 1998 An atmospheric undular bore along the Texas coast. *Mon. Weath. Rev.* **126**, 1098–1100.

El, G. A. 2005 Resolution of a shock in hyperbolic systems modified by weak dispersion. *Chaos* **15**, 037103.

El, G. A., Grimshaw, R. H. J. & Smyth, N. F. 2006 Unsteady undular bores in fully nonlinear shallow-water theory. *Phys. Fluids* **18**, 027104.

El, G. A., Grimshaw, R. H. J. & Smyth, N. F. 2009 Transcritical shallow water flow past topography: finite-amplitude theory. *J. Fluid Mech.* **640**, 187–215.

El, G. A., Khodorovskii, V. V. & Tyurina, A. V. 2003 Determination of boundaries of unsteady oscillatory zone in asymptotic solutions of non-integrable dispersive wave equations. *Phys. Lett.* A **318**, 526–536.

El, G. A., Khodorovskii, V. V. & Tyurina, A. V. 2005 Undular bore transition in bi-directional conservative wave dynamics. *Physica* D **206**, 232–251.

Favre, H. 1935 *Etude Théoretique et Éxperimentale des Ondes de Translation dans les Canaux Decouverte*. Dunod.

Grimshaw, R. 2002 Internal solitary waves. In *Environmental Stratified Flows*, chap. 1, pp. 1–28. Kluwer.

Grimshaw, R., Pelinovsky, D., Pelinovsky, E. & Slunyaev, A. 2002 The generation of large-amplitude solitons from an initial disturbance in the extended Korteweg–de Vries equation. *Chaos* **12**, 1070–1076.

Gurevich, A. V. & Pitaevskii, L. P. 1974 Nonstationary structure of a collisionless shock wave. *Sov. Phys. JETP* **38**, 291–297.

Holloway, P., Pelinovsky, E. & Talipova, T. 2001 Internal tide transformation and oceanic internal solitary waves. In *Environmental Stratified Flows*, chap. 2, pp. 29–60. Kluwer.

Hosegood, P. & van Haren, H. 2004 Near-bed solibores over the continental slope in the Faroe-Shetland channel. *Deep-sea Res.* II **51**, 2943–2971.

Kamchatnov, A. N. 2000 *Nonlinear Periodic Waves and Their Modulations – An Introductory Course*. World Scientific.

Klemp, J. B., Rotunno, R. & Skamarock, W. C. 1994 On the dynamics of gravity currents in a channel. *J. Fluid Mech.* **269**, 169–198.

Klemp, J. B., Rotunno, R. & Skamarock, W. C. 1997 On the propagation of internal bores. *J. Fluid Mech.* **331**, 81–106.

Laget, O. & Dias, F. 1997 Numerical computation of capillary-gravity interfacial solitary waves. *J. Fluid Mech.* **349**, 221–251.

Li, M. & Cummins, P. F. 1998 A note on hydraulic theory of internal bores. *Dyn. Atmos. Oceans* **28**, 1–7.

Liska, R., Margolin, L. & Wendroff, B. 1995 Nonhydrostatic two-layer models of incompressible flow. *Comput. Math. Appl.* **29**, 25–37.

MacKinnon, J. A. & Gregg, M. C. 2003 Shear and baroclinic energy flux on the summer New England shelf. *J. Phys. Oceanogr.* **33**, 1462–1475.

Milewski, P. A., Tabak, E. G., Turner, C. V., Rosales, R. R. & Menzaque, F. E. 2004 Nonlinear stability of two-layer flows. *Commun. Math Sci.* **2**, 427–442.

Miyata, M. 1985 An internal solitary wave of large amplitude. *La Mer* **23**, 43–48.

Pearce, J. D. 2009 Dispersive phenomena in extended shallow water models of geophysical flows. PhD thesis, Senate House Library, University of London, London, UK.

Rottman, J. W. & Grimshaw, R. 2002 Atmospheric internal solitary waves. In *Environmental Stratified Flows*, chap. 3, pp. 61–88. Kluwer.

Rottman, J. W. & Simpson, J. E. 1983 Gravity currents produced by instantaneous releases of a heavy fluid in a rectangular channel. *J. Fluid Mech.* **135**, 95–110.

Rottman, J. W. & Simpson, J. E. 1989 The formation of internal bores in the atmosphere: a laboratory model. *Q. J. R. Meteorol. Soc.* **115**, 941–963.

Sandstrom, H. & Quon, C. 1993 On time-dependent, two-layer flow over topography. Part I. Hydrostatic approximation. *Fluid Dyn. Res.* **11**, 119–137.

Shin, J. O., Dalziel, S. B. & Linden, P. F. 2005 Gravity currents produced by lock exchange. *J. Fluid Mech.* **521**, 1–34.

Su, C. H. & Gardner, C. S. 1969 Korteweg-de Vries equation and generalizations. Part III. Derivation of the Korteweg-de Vries equation and Burgers equation. *J. Math. Phys.* **10**, 536.

Whitham, G. B. 1965 Non-linear dispersive waves. *Proc. R. Soc. Lond., Ser.* A **283**, 238–291.

Wood, I. R. & Simpson, J. E. 1984 Jumps in layered miscible fluids. *J. Fluid Mech.* **140**, 215–231.

Zahibo, N., Slunyaev, A., Talipova, T., Pelinovsky, E., Kurkin, A. & Polukhina, O. 2007 Strongly nonlinear steepening of long interfacial waves. *Nonlinear Process. Geophys.* **14**, 247–256.